Structural and Acidic Properties of Mordenite. An ab Initio Density-Functional Study

T. Demuth,*,† J. Hafner,† L. Benco,† and H. Toulhoat‡

Institut für Materialphysik and Center for Computational Materials Science, Universität Wien, Sensengasse 8, A-1090 Wien, Austria, and Molecular Modeling and Computational Chemistry Division, Institut Français du Pétrole, 1 & 4 Avenue de Bois-Préau, F-92852 Rueil-Malmaison Cedex, France

Received: October 29, 1999; In Final Form: February 10, 2000

The effects of the Si → Al substitution on the structure of the siliceous framework and the structure and vibrational properties of Brønsted acid sites in mordenite have been studied using density-functional theory, both in the local-density approximation and including generalized gradient corrections to the exchange-correlation functional. The substitution induces a substantial local deformation of the polytetrahedral geometry of pure-silica mordenite. Also the counterions have a strong influence on the geometry of the framework. Protonation of bridging (Si)−O−(Al) oxygen atoms is accompanied by a further local distortion of the structure. Changes in the bond lengths remain well localized to the nearest neighborhood of the perturbation center; O−H stretching frequencies of acidic protons were calculated in both harmonic and anharmonic approximations, indicating a rather complex relationship among stability, frequencies, and local environment of the Brønsted acid sites.

I. Introduction

Zeolites are microporous aluminosilicates that are industrially important for their catalytic and molecular sieving properties. Their network of cavities and channels allows them to accommodate even moderately large molecules, and the presence of Al-substituted tetrahedral sites, with an associated H^+ being bound to a nearby O atom to maintain charge neutrality, results in acidic properties useful in catalysis.[1,2] A further important factor determining the catalytic activity of zeolites is the confinement of the reacting molecules within their pores. Inside a zeolite a sorbate molecule moves in a periodic potential determined by its structural features, i.e., by the geometry of the aluminosilicate framework and the location of extraframework cations.

Because of the large unit cell of most zeolites (varying between about 50 and more than 300 atoms), nearly all ab initio studies of these materials have been performed on small clusters representing the catalytically active acid site and part of the surrounding framework.[3−6] Only recently local-density-functional theory (LDFT) has been developed to a point where the geometry and electronic properties of zeolites (and in particular the structure of the acid sites) can be studied. However, so far the investigations have been restricted to zeolites with a relatively modest size of the unit cell such as chabazite (36 atoms/cell),[7,8] sodalite[9] (36 atoms/cell), offretite (54 atoms/cell),[10,11] or the related silicoaluminophosphate HSAPO-34 (36 atoms/cell).[8,12,13] The only attempt to extend these studies to a zeolite widely used in industrial processes was made by Kessi and Delley,[14] who presented a structure relaxation of pure-silica mordenite (144 atoms/cell), at a fixed volume and shape of the unit cell. Periodic Hartree−Fock studies have been performed for chabazite.[15,16] Using reduced basis sets, White and Hess have extended the HF studies to mordenite[17] and zeolite ZSM-5 (288 atoms/cell).[18] A number of studies have been devoted to a comparison between periodic and cluster approaches, in both LDFT and HF.[14,16,19]

Dehydrated Na-mordenite has the composition $Na_8Al_8Si_{48}O_{96}$.[20,21] Natural mordenite may have a slightly different Al/Si ratio; the extraframework cations are a mixture of alkaline (Na, K) and alkaline-earth (Mg, Ca, Sr) ions. In addition, the pores contain a large number (up to 30) of water molecules.[22] The mordenite structure is stable to acid leaching, allowing almost all aluminum to be removed and essentially pure-silica mordenite to be produced.[23]

The orthorhombic unit cell of natural mordenite has the lattice parameters[22] $a = 18.09$ Å, $b = 20.52$ Å, and $c = 7.52$ Å. Two types of cavities are present in the structure: (i) a main channel circumscribed by twelve-membered rings (i.e., by rings containing twelve silicon atoms) running along the *c* axis, measuring 6.7 Å × 7.9 Å; (ii) smaller channels surrounded by eight-membered rings running along the *b* direction and measuring 2.6 Å × 5.7 Å. Since these narrower channels allow a diffusion of only rather small molecules, they are often referred to as "side pockets" that can be entered only from the main channel but do not provide a connection between adjacent channels. A projection of the mordenite lattice along the *c* axis is shown in Figure 1. X-ray diffraction studies have been performed for a variety of natural and synthetic mordenites.[20−28] For the purely siliceous framework, the space group is *Cmcm*, but the extraframework ions break the symmetry. Alberti et al.[22] have argued that for natural mordenite the acentric space group $Cmc2_1$ provides a more accurate description of the structure. In dehydrated K- and Ba-exchanged mordenites, the symmetry is lowered from *Cmcm* to *Pbcn*.[29,30] The different symmetries reflect the preference of different counterions for different sites in the cavities; this is of course intimately coupled to the distribution of the Al ions over the available tetrahedral sites. It has been argued that in mordenite Al atoms are preferentially located on the T3 and T4 sites forming the small four-membered rings of the structure (see Figure 1).[22] This would seem to

* Corresponding author. E-mail: Thomas.Demuth@univie.ac.at. Phone: +43-1-4277-51403. Fax: +43-1-4277-9514.

† Universität Wien.

‡ Institut Français du Pétrole.

10.1021/jp993843p CCC: $19.00
Published on Web 04/25/2000

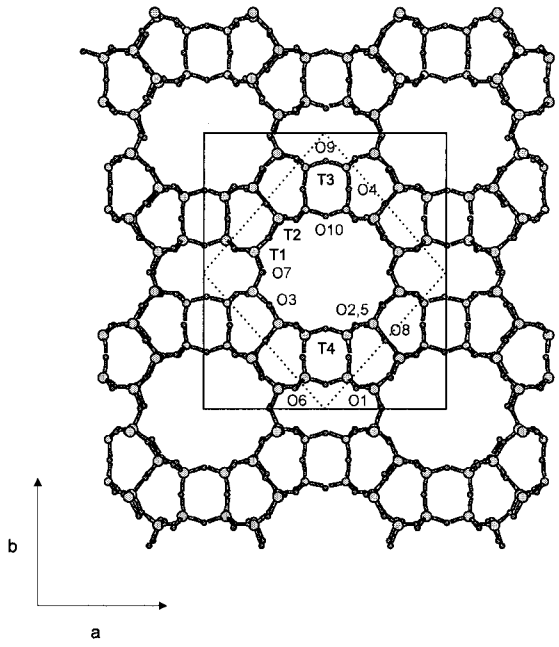

Figure 1. Projection of the mordenite framework along the *c* axis, presenting a view along the main channel (twelve-membered ring) and showing also the side pockets (eight-membered rings). The four inequivalent tetrahedral sites labeled T1 to T4 (T = Si or Al) are shown by the larger light gray spheres. Oxygen atoms are represented by smaller dark spheres and numbered O1 to O10. Note that O2 and O5 sites are superposed in a projection along the *c* axis (see also Figure 3). The solid frame shows the conventional centrosymmetric orthorhombic unit cell, the dashed frame the primitive unit cell.

correlate with the positions of the counterions reported for the Na-exchanged mordenite: according to Meier[20] there are two inequivalent Na positions; Na1 lies in the center of the eight-membered rings (i.e., outside the main channels), and Na2 is probably situated within the main channel. Schlenker et al.[25] suggest that the Na2 ions are located at the center of the eight-membered rings opening the entrance from the main channel to the side pockets. Ab initio geometry optimizations certainly offer a possibility to obtain precise information on the location of the counterions.

The catalytic properties of zeolites arise from the creation of acid sites: Starting from a pure-silica zeolite, one of the Si atoms is replaced by Al, and to compensate for the charge difference, an H atom is attached to one of the oxygens adjacent to the Al atom. Alternatively, starting, e.g., from Na-mordenite, one or more of the counterions are eliminated, and instead a hydrogen atom is added to an oxygen atom adjacent to one of the Al sites. The acidity of the hydroxyl groups depends in a crucial way on the structural properties of the acid sites[31−33] which cannot, however, be determined by experiment. Experimental characterization of the acid sites is mostly based on infrared spectroscopy identifying different vibrational bands attributed to the acid sites. Quite generally a lower O−H stretching frequency is associated with a higher acidity, because it reflects a weaker O−H bond. The correlations between the structural and dynamical properties of acid sites, however, remain to be explored.

In the present paper we report local-density-functional studies of pure-silica mordenite, Na-mordenite, and H-mordenite. Full structural optimizations have been performed in all three cases, using both local and gradient-corrected exchange-correlation functionals. For Na-mordenite, the distortions of the framework resulting from the substitution $Si^{4+} \rightarrow Al^{3+} + Na^{+}$ and the equilibrium positions of the Na^{+} counterions have been studied in detail. For H-mordenite the structure, stability, and dynamical properties of possible acid sites have been analyzed.

II. Methods

Ab initio total-energy calculations have been performed using the Vienna ab initio simulation package VASP.[34−36] VASP performs an iterative solution of the Kohn−Sham equations of density-functional theory, based on the minimization of the norm of the residual vector to each eigenstate and an efficient charge density mixing. For the exchange-correlation functional both the local-density approximation (LDA) in the form of the Perdew−Zunger parametrization[37] of the quantum Monte Carlo simulations of Ceperley and Alder[38] and gradient-corrected functionals in the form of the generalized gradient approximation (GGA) of Perdew and Wang et al.[39,40] have been used. The calculations are performed in a plane-wave basis set, using the projector-augmented wave (PAW) method originally developed by Blöchl[41] and recently adapted by Kresse and Joubert.[42] In this connection, the close similarity between the PAW and plane-wave calculations using ultrasoft pseudopotentials[43,44] should be noted; for details see ref 42. The particular advantage of the PAW method over the ultrasoft pseudopotentials is that the pseudization of the augmentation charge can be avoided. The calculations have been performed using a relatively low plane-wave cutoff of 300 eV, due to the use of a soft oxygen potential. Both the plane-wave cutoff and the parameters defining the projectors have been carefully tested in a series of calculations on a large number of silica polytypes, ranging from tridymite to high-pressure post-stishovite phases,[45,46] and in previous studies of chabazite and HSAPO-34,[8,12] exploiting the one-to-one correspondence between projector-augmented waves and ultrasoft pseudopotentials. For the large unit cell of mordenite it is legitimate to restrict the Brillouin-zone sampling to the Γ point, using a modest smearing of the eigenvalues to improve total-energy convergence.

The structural optimization was performed in two steps: First, the cell shape and internal parameters were relaxed at fixed volumes using a quasi-Newton algorithm and analytical Hellmann−Feynman forces acting on the atoms and stresses on the unit cell. Structural parameters were considered to be converged if the forces on the atoms became smaller than 0.1 eVÅ^{-1}. These calculations were repeated for a series of fixed volumes, leading to a $E(V)$ curve. The equilibrium volume was determined via a polynomial fit to the $E(V)$ curve, and the final structural parameters were derived from a further fixed-volume relaxation at the zero-pressure volume. This procedure avoids problems related to the incompleteness of the plane-wave basis set with respect to variations of the volume (Pulay stress). The bulk modulus was determined for the curvature of the $E(V)$ curve at zero pressure.

The vibrational analysis concentrated on the determination of the O−H stretching frequencies which characterize the reactivity of the acid site and which have been examined in detail by infrared spectroscopy. The stretching frequencies were calculated using both classical and quantum mechanical methods. The former approach is based on the numerical derivatives of the analytical forces induced by small positive (stretching) and negative (compression) deformations of the O−H bond length. Harmonic frequencies were derived from the derivatives at the equilibrium bond length, calculated for small deformations. Anharmonic O−H stretching frequencies were calculated by fitting the potential energy curve by a Morse potential over a somewhat wider range of deformations. We have performed both calculations with a full relaxation of all atoms, and

TABLE 1: Lattice Constants, Bulk Moduli B_0 and Pressure Derivative B_0' Calculated for the Pure-Silica and Na-Mordenite in the Local-Density Approximation (LDA) and Using Generalized Gradient Corrections (LDA + GGA)[a]

	space group		a (Å)	b (Å)	c (Å)	V (Å^3)	B_0 (GPa)	B_0'
pure-silica mordenite	*Cmcm*	LDA	18.101	20.501	7.526	58.18	74.04	4.59
	Cmcm	GGA	18.260	20.706	7.606	59.91	68.07	3.80
Na-mordenite	$P2_1/m$	LDA	18.284	20.368	7.519	58.33	71.56	4.32
	$P2_1/m$	GGA	18.487	20.643	7.616	60.55	64.32	3.82
natural mordenite[b]	$Cmc2_1$		18.094	20.516	7.524	58.185		
ion-exch mordenite[c]	*Cmcm*		18.089	20.412	7.504	57.72		
dehydr mordenite[c]	*Cmcm*		17.941	20.276	7.482	56.70		
dehydr. mordenite[d]	*Pbcn*		17.92	20.31	7.480	56.71		
hydrogenat mordenite[e]	*Cmcm*		18.223	20.465	7.531	58.51		

[a] For comparison the lattice constants determined by Alberti et al. (ref 22) for natural mordenite, by Ito and Saito (ref 28) for hydrated and dehydrated ion-exchanged mordenite, and by Schlenker et al. (refs 25 and 26) for dehydrated sodium-exchanged and dehydrated protonated mordenite are given. [b] Reference 22. [c] Reference 28. [d] Reference 25. [e] Reference 26.

assuming a rigid framework. A small difference between both approaches would demonstrate that the O−H stretching mode is essentially a pure eigenmode which couples only very weakly to the eigenmodes of the zeolite framework.[47] Due to the small mass of the hydrogen atom, the quantum character of the dynamics has to be considered. In the present case we have determined the one-dimensional potential energy surface for the O−H stretching using ab initio LDF calculations and solved numerically the Schrödinger equation for the H atom moving in this potential using the method proposed by Ugliengo.[48] The anharmonicity constants $\omega_e\chi_e$ are estimated from the frequencies of the two lowest eigenmodes

$$2\omega_e\chi_e = 2\omega_{01} - \omega_{02} \quad (1)$$

and the harmonic frequencies are determined by the relation

$$\omega_e = \omega_{01} + 2\omega_e\chi_e \quad (2)$$

This determination of the anharmonicity follows essentially the same principles that are used in the analysis of the experimental data.

III. Structure of Pure-Silica Mordenite

The crystal structure of the purely siliceous mordenite was optimized with respect to the lattice parameters and the internal coordinates of the atoms, assuming the orthorhombic *Cmcm*-D_{2h}^{17} symmetry used by Meier[20] in his original refinement of dehydrated mordenite. It is generally assumed that only the extraframework atoms break the *Cmcm* symmetry. A particular feature of the structure is the presence of a Si−O−Si bond angle of 180°. Straight Si−O−Si bonds are generally energetically unfavorable in silica polymorphs and in silicates (cf. our discussion of the silica polymorphs[45]). The cell dimensions given by Alberti et al.[22] are a = 18.094 Å, b = 20.516 Å, and c = 7.524 Å; the cell contains 48 silicon atoms and 96 oxygen atoms.

Our results for the optimized cell parameters are given in Table 1. The lattice constants calculated in the LDA are in excellent agreement with the values resulting from the refinement of Alberti et al.[22] performed on natural mordenite with the stoichiometry $Na_{1.5}K_{2.8}Ca_{2.1}Al_9Si_{39}O_{96}$ and containing about 29 water molecules per cell. Ito and Saito[28] have reported a structural refinement for ion-exchanged mordenite with composition $Na_{1.4}Ca_{2.9}Al_{7.2}Si_{40.8}O_{96}$ and an unspecified number of water molecules, yielding almost identical cell parameters. Ito and Saito determine also the cell dimensions for dehydrated mordenite. Compared to the hydrated sample, the lattice constants are reduced by −0.82% along the a axis, −0.66% along the b axis, and −0.3% along the c axis; the average volume per SiO_2 unit is reduced by −1.77%. Schlenker et al.[25] analyzed both dehydrated sodium-exchanged and protonated mordenite. The cell dimensions for the sodium-exchanged structure are lower than for the hydrogen mordenite. The largest decrease occurs for the lattice constant a by −1.66%.

Repeating the calculations with the gradient-corrected exchange-correlation functional leads to an increase of all lattice constants by about 1%. This means that compared to dehydrated mordenite[28] the LDA overestimates the equilibrium volume by about 2.6%, including the GGC by about 5.7%. In earlier ab initio calculations for chabazite and HSAPO-34, a somewhat smaller overestimate of the volume calculated in the LDA + GGA was found.[8] Also compared to ab initio LDF calculations for the more closed-packed silica polymorphs, we find a somewhat greater tendency to an overestimate of the equilibrium volume. We have also calculated the bulk modulus B_0 and its pressure derivative B_0'. The value of B_0 = 74.04 GPa for mordenite calculated in the LDA lies about halfway between the moduli calculated for the hardest and softest tetrahedrally coordinated silica polymorphs (B_0 = 13 GPa for α-cristobalite, B_0 = 140 GPa for β-tridymite) and is comparable to that of coesite.[45] Since the volume per SiO_2 unit is about twice as large as in an average silica polymorph, this shows that the zeolite framework retains a certain stiffness despite the large cavities.

The optimized internal parameters for the pure-silica mordenite are compiled in Table 2, where they are compared with the experimental results of Alberti et al.[22] In both the LDA and the LDA + GGA we find very good agreement between theory and experiment; the equilibrium coordinates are slightly more accurate than those determined by Kessi and Delley[14] in a fixed-volume relaxation. The better agreement is probably due to the relaxation of the cell parameters in our calculation. Internal parameters calculated in the LDA and GGA disagree only in the fourth digit; hence, the effect of the nonlocal corrections is limited to a uniform expansion of the lattice.

Table 3 summarizes the results for the Si−O bond lengths and for the O−Si−O and Si−O−Si bond angles, respectively. On average, the bond lengths calculated within the LDA agree with experiment within 0.02 Å. However, the rms deviations of the individual bond lengths from the average value are considerably smaller for the theoretical structure: for the structure determined by Alberti et al.,[22] the difference between the longest and shortest Si−O bond is 0.062 Å, Ito and Saito[28] find a maximal difference of even 0.081 Å, and Schlenker et al.[26] report a difference of 0.042 Å. In the LDA the largest difference is only 0.016 Å. A similar result is found for the intratetrahedral angles around the Si-atoms: whereas for both theory and experiment the average value is very close to the ideal tetrahedral angle of 109.43°, the largest deviation is 3.9° for the structure of Alberti et al., 4.7° for the structure of Ito

TABLE 2: Optimized Fractional Coordinates of Pure-Silica Mordenite $Si_{48}O_{96}$ (Space Group Symmetry *Cmcm*), Compared with the Results of the Structure Refinement by Alberti et al. (Reference 22)

site	symmetry		*x*	*y*	*z*
T1	16*h*	LDA	0.3030	0.0729	0.0429
		GGA	0.3026	0.0731	0.0428
		exptl	0.3007	0.0724	0.0412
T2	16*h*	LDA	0.3041	0.3099	0.044
		GGA	0.3043	0.3097	0.0450
		exptl	0.3037	0.3088	0.0461
T3	8*g*	LDA	0.0862	0.3820	0.25
		GGA	0.0863	0.3821	0.25
		exptl	0.0870	0.3841	0.25
T4	8*g*	LDA	0.0857	0.2263	0.25
		GGA	0.0857	0.2264	0.25
		exptl	0.0867	0.2278	0.25
O1	16*h*	LDA	0.1245	0.4111	0.4261
		GGA	0.1245	0.4110	0.4267
		exptl	0.1243	0.4170	0.4287
O2	16*h*	LDA	0.1225	0.1959	0.4256
		GGA	0.1224	0.1959	0.4258
		exptl	0.1226	0.1954	0.4254
O3	16*h*	LDA	0.2370	0.1222	0.9955
		GGA	0.2364	0.1221	0.9935
		exptl	0.2362	0.1224	0.9865
O4	8*g*	LDA	0.0968	0.3041	0.25
		GGA	0.0968	0.3042	0.25
		exptl	0.0958	0.3064	0.25
O5	8*g*	LDA	0.1729	0.1926	0.75
		GGA	0.1722	0.1935	0.75
		exptl	0.1696	0.1960	0.75
O6	8*g*	LDA	0.1764	0.4201	0.75
		GGA	0.1772	0.4200	0.75
		exptl	0.1778	0.4208	0.75
O7	8*e*	LDA	0.2245	0.5	0.5
		GGA	0.2249	0.5	0.5
		exptl	0.2321	0.5	0.5
O8	8*d*	LDA	0.25	0.25	0.5
		GGA	0.25	0.25	0.5
		exptl	0.25	0.25	0.5
O9	4*c*	LDA	0.0	0.4007	0.25
		GGA	0.0	0.4012	0.25
		exptl	0.0	0.4067	0.25
O10	4*c*	LDA	0.0	0.2082	0.25
		GGA	0.0	0.2081	0.25
		exptl	0.0	0.2050	0.25

and Saito, 2.4° for the structure of Schlenker et al., and only 1.4° for the structure calculated in the LDA. The largest differences between theory and experiment are found for the Si−O−Si bond angles. Differences of up to 8.3° are found around the sites O1, O5, O7, O9, and O10 (except around O4 the experimentally determined angles are more acute), whereas the angles determined for the other sites agree with experiment within 1−2°. It is remarkable that the larger deviations in the Si−O−Si angles correlate with larger discrepancies in the Si−O bond lengths for the corresponding oxygen sites. This shows that the structure optimization leads to a more regular polytetrahedral framework than the experimental structural refinement. This conclusion is also corroborated by a calculation of the deformation parameters. Complete tables of the deformation parameters can be found in the Supporting Information (see Figure 1S and Table IS). Of course this is to be expected, because the experimental analysis has been performed on a sample with an at least partially random Si → Al substitution.

A particular consequence of the *Cmcm* symmetry is the 180° bond angle around the O8 site. In the experimental structure this leads to a somewhat compressed Si2−O8 bond, whereas in the relaxed structure the straight Si−O−Si bond can be accommodated without an additional strain on the bond length. Our result that the structural optimization of mordenite leads

TABLE 3: Interatomic Distances (Å) and Bond Angles (deg) in the Mordenite Framework, As Calculated for the Pure-Silica Case in the LDA and GGA Approximations and Compared to the Experimental Results of Alberti at al. (Reference 22), Ito and Saito (Reference 28), and Schlenker et al. (Reference 26)[a]

	LDA	GGA	exptl[22]	exptl[28]	exptl[26]
(a) Bond Lengths (Å)					
T1−O1	1.612	1.630	1.614	1.609	1.605
T1−O3	1.604	1.622	1.607	1.616	1.593
T1−O6	1.608	1.623	1.624	1.610	1.609
T1−O7	1.609	1.628	1.629	1.625	1.613
mean	1.608	1.626	1.618	1.615	1.605
rms	0.286	0.334	0.855	0.636	0.748
T2−O2	1.605	1.619	1.616	1.606	1.608
T2−O3	1.606	1.622	1.604	1.588	1.591
T2−O5	1.601	1.617	1.611	1.610	1.608
T2−O8	1.607	1.622	1.587	1.583	1.587
mean	1.604	1.620	1.604	1.597	1.598
rms	0.227	0.212	1.096	1.147	0.960
T3−O1	1.610	1.628	1.649	1.664	1.626
T3−O4	1.608	1.624	1.602	1.639	1.612
T3−O9	1.606	1.625	1.641	1.656	1.627
mean	1.608	1.626	1.635	1.656	1.622
rms	0.165	0.178	1.947	1.020	0.622
T4−O2	1.606	1.623	1.614	1.620	1.611
T4−O4	1.608	1.623	1.620	1.588	1.585
T4−O10	1.596	1.610	1.637	1.616	1.613
mean	1.604	1.620	1.621	1.611	1.605
rms	0.469	0.562	0.941	1.337	1.157
(b) Intratetrahedral Bond Angles (deg)					
O1−T1−O3	110.9	110.9	113.0	112.9	110.9
O1−T1−O6	108.8	108.9	107.1	107.9	107.4
O1−T1−O7	109.3	109.3	109.2	109.6	109.2
O3−T1−O6	109.4	109.7	111.5	111.1	111
O3−T1−O7	108.0	107.7	105.6	104.8	107.8
O6−T1−O7	110.4	110.2	110.5	110.7	110.5
mean	109.5	109.4	109.5	109.5	109.5
rms	0.962	1.009	2.526	2.589	1.447
O2−T2−O5	108.8	108.6	106.5	106.4	107
O2−T2−O3	110.1	110.0	109.4	109.6	109.9
O2−T2−O8	109.2	109.3	110.0	110.5	110.3
O3−T2−O5	109.3	109.4	109.5	109.6	109.4
O3−T2−O8	109.8	110.1	111.1	107.7	110.1
O5−T2−O8	109.5	109.4	110.2	110.8	110.0
mean	109.4	109.5	109.4	109.1	109.4
rms	0.419	0.495	1.431	1.559	1.129
O1−T3−O1	110.8	111.3	109.3	109.8	109.3
O1−T3−O4	108.4	108.3	111.5	111.4	110.5
O1−T3−O9	109.3	109.0	106.1	105.7	107.4
O4−T3−O9	110.6	110.9	112.1	112.5	111.6
mean	109.5	109.5	109.4	109.4	109.4
rms	0.948	1.195	2.513	2.743	1.594
O2−T4−O2	110.8	110.9	109.7	108.1	109.1
O2−T4−O10	108.2	108.0	105.5	112.9	108.3
O2−T4−O4	109.5	109.5	111.6	111.6	109.6
O4−T4−O10	110.6	110.8	112.4	106.2	112.0
mean	109.5	109.4	109.4	110.5	109.5
rms	1.022	1.164	2.863	2.522	1.245
(c) Bond Angles around Oxygen Sites (Intertetrahedral Bond Angles) (deg)					
T1−O1−T3	150.9	150.5	145.8	144.9	149.7
T1−O3−T2	158.8	158.1	158.9	157.5	159.3
T1−O6−T1	151.3	152.0	150.5	153.1	149.4
T1−O7−T1	143.9	144.0	137.3	135.6	143.2
T2−O2−T4	146.2	146.1	144.5	145.0	146.3
T2−O5−T2	149.7	149.1	144.4	143.1	146.6
T2−O8−T2	180	180	180	180	180
T3−O4−T4	166.0	166.0	168.5	168.7	168.4
T3−O9−T3	152.5	151.8	147.2	145.0	147.8
T4−O10−T4	153.1	152.8	146.8	146.8	148.2

[a] Note that the T3 and T4 sites are located on mirror planes so that only four O−T−O angles need to be listed.

to a structure with smaller distortions of the local tetrahedral units than those present in the experimentally determined structure agrees with similar results obtained by Campana et al.[10,11] and by Kessi and Delley[14] for offretite and correlates rather well with the conclusions of White and Hess,[17,18] who performed periodic Hartree−Fock total-energy calculations for a variety of experimentally reported mordenite structures. The highest total energy was reported for the structure determined by Meier,[20] leading to the widest spread of Si−O bond lengths and O−Si−O bond angles; the lowest total energy was reported for the framework derived by Schlenker et al.[26] for the acid-treated hydrogen mordenite; showing the smallest standard deviations of the bond lengths and angles from the mean values (energy difference 186 kcal/mol per unit cell); cf. also Table 3.

These standard deviations are, however, still larger than those resulting from our structural optimization. The fact that a reduced spread of bond lengths and angles increases structural stability is supported by empirical observations of Gibbs[49] and Petrovic and Navrotsky[50] based on a comparison of the structures and thermal stabilities of various siliceous zeolites.

IV. Structure of Na-Mordenite

In the next step we consider the structure of mordenite with an average Al/Si ratio of 1/5. Therefore, 8 out of 48 Si atoms have to be substituted by Al atoms, and the unit cell must contain 8 monovalent counterions. As mentioned before the mordenite structure has four distinct tetrahedral sites (see Figure 1). From an experimental point of view it is only possible to determine the average concentration of Al in certain tetrahedral sites,[22] indicating a significant partial Si/Al ordering in mordenite. The T3 and to a lesser extent the T4 site are the tetrahedral sites richest in Al; they constitute the four-membered rings in the structure. The occurrence of Al in the four-membered ring in mordenite was also shown by Derouane and Fripiat.[51] According to the empirical Löwenstein rule[52] that forbids the presence of Al atoms in neighboring tetrahedra, we decided for our starting configuration to substitute four of the silicon atoms on the T3 and four on the T4 sites by aluminum to achieve an Al/Si ratio of 1/5 (see Table 4). To retain charge neutrality, it is therefore necessary to include eight sodium atoms forming extraframework cations in the structure. The experimental refinement of the structure cannot give a completely reliable distribution on the extraframework sites. Only four of the sodium ions have been definitely located (Na1). These lie in the center of the small eight-membered ring. For the remaining four sodium (Na2) ions we decided to put them in the center of the second main channel (side pockets) (see Figure 3). This position is comparable to site B proposed in ref 22. After a full structural relaxation, the positions of these sodium atoms are different (see Figure 3) from the starting centered position. The sodium atoms are shifted away from the high-symmetry position to an off-center configuration; however, they remain in the plane of the eight-membered ring. The largest decrease of the Na2−O distance occurs for the Na2−O5 pair by ∼0.8 Å. This final position could be identified with position D of ref 22. Note that there is of course an equivalent position on the other side of the ring.

A. Crystal Structure. From a crystallographic point of view it is important that the Si → Al substitution and the introduction of counterions break the symmetry of the purely siliceous lattice, which is lowered to monoclinic $P2_1/m$ symmetry. We find that the deviations of the cell parameters from the starting orthorhombic space group are very small; e.g., the monoclinic angle β is around 91°. To determine the equilibrium structure, we performed energy vs volume calculations allowing for a relaxation of all lattice parameters and all the atomic coordinates within the unit cell. Therefore, at a fixed volume this means that 45 structural parameters have to be refined to determine the equilibrium structure. The energy vs volume curves of both types ("ideal" and substituted mordenite) are shown in Figure 2 in both LDA and GGA approximations; the optimized cell parameters are given in Table 1. The changes of the cell parameters and of the internal coordinates as a function of volume are extremely small. In the LDA the difference between the equilibrium volumes of purely siliceous and Al-substituted

TABLE 4: Optimized Fractional Coordinates for Mordenite $Na_8Al_8Si_{40}O_{96}$[a]

atom	$P2_1/m$ position	LDA			GGA		
		x	*y*	*z*	*x*	*y*	*z*
Na1	2c[b]	0.0	0.5	0.0	0.0	0.5	0.0
Na2	2e[b]	0.5352	0.3132	0.25	0.5336	0.3129	0.25
Al3	2e[b]	0.0843	0.6119	0.75	0.0845	0.6138	0.75
Al4	2e[b]	0.0841	0.2250	0.25	0.0842	0.2241	0.25
Si1(1)	4f[b]	0.3026	0.0690	0.0455	0.3027	0.0697	0.0455
Si1(2)	4f[b]	0.3031	0.0726	0.0424	0.3030	0.0727	0.0423
Si2(1)	4f[b]	0.3024	0.3092	0.0486	0.3025	0.3091	0.0474
Si2(2)	4f[b]	0.3021	0.3124	0.0401	0.3020	0.3122	0.0404
Si3	2e[b]	0.0851	0.3875	0.25	0.0859	0.3862	0.25
Si4	2e[b]	0.0861	0.7741	0.75	0.0861	0.7745	0.75
O1(1)	4f[b]	0.1239	0.4173	0.4288	0.1240	0.4169	0.4288
O1(2)	4f[b]	0.1191	0.4231	0.4437	0.1198	0.4208	0.4433
O2(1)	4f[b]	0.1211	0.1940	0.4431	0.1214	0.1935	0.4432
O2(2)	4f[b]	0.1256	0.1931	0.4267	0.1250	0.1938	0.4281
O3(1)	4f[b]	0.2416	0.1232	0.9747	0.2417	0.1232	0.9788
O3(2)	4f[b]	0.2429	0.1234	0.9601	0.2413	0.1232	0.9671
O4(1)	2e[b]	0.0845	0.3102	0.25	0.0867	0.3093	0.25
O4(2)	2e[b]	0.0956	0.3039	0.25	0.0963	0.3027	0.25
O5(1)	2e[b]	0.1844	0.1799	0.75	0.1839	0.1814	0.75
O5(2)	2e[b]	0.1645	0.1987	0.75	0.1659	0.1981	0.75
O6(1)	2e[b]	0.1708	0.4363	0.75	0.1710	0.4337	0.75
O6(2)	2e[b]	0.1876	0.4093	0.75	0.1858	0.4120	0.75
O7	4f[b]	0.2313	0.5007	0.4808	0.2303	0.5006	0.4852
O8(1)	4f	0.25	0.25	0.5	0.25	0.25	0.5
O8(2)	4f	0.25	0.75	0.0	0.25	0.75	0.0
O9	2e[b]	0.0049	0.4220	0.25	0.0051	0.4194	0.25
O10	2e[b]	0.0059	0.1995	0.25	0.0057	0.1996	0.25

[a] The space group is lowered from *Cmcm* to $P2_1/m$ due to substitution of aluminum. All experimental structural refinements assume that the *Cmcm* symmetry of the pure-silica structure is not broken by the Si → Al substitution and the introduction of counterions [b] Add (1/2, 1/2, 0).

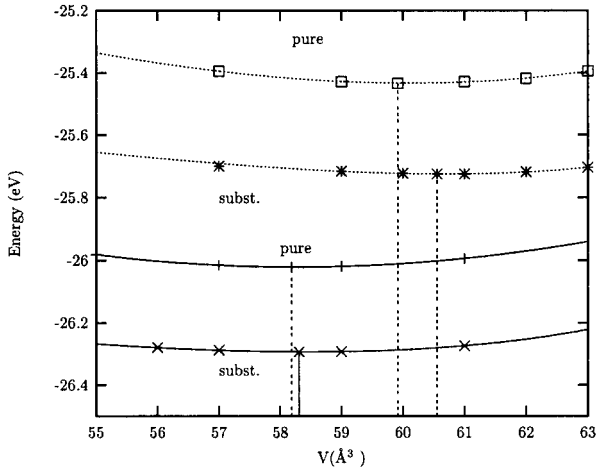

Figure 2. Energy as a function of the volume per SiO_2 unit for ideal and Al-substituted mordenite. The full lines represent the LDA and the broken lines the GGA results. The vertical lines indicate the equilibrium volumes. Note that the GGA energies have been shifted by 1.5 eV.

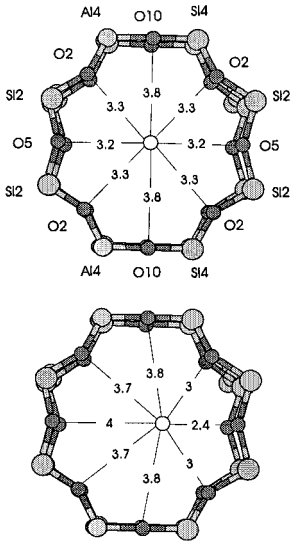

Figure 3. Coordination around the Na2 atom located in the plane of the eight-membered ring. The first figure shows the starting centered configuration, the figure below the final and off-center position of the sodium atom.

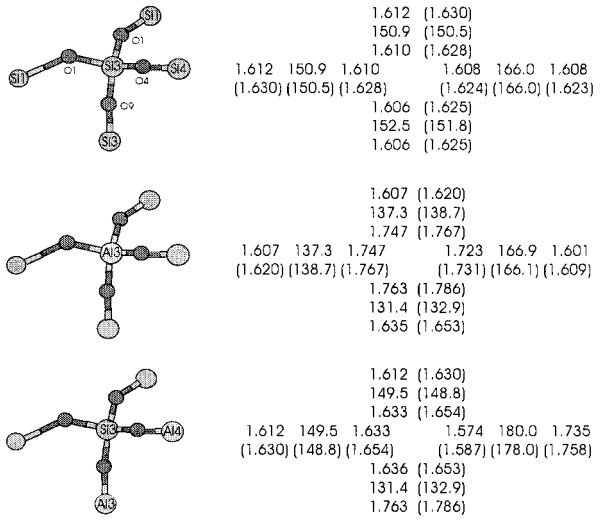

Figure 4. Bond lengths (Å) and T−O−T angles for the T3 site: top, ideal mordenite; middle, Na-exchanged Al-substituted mordenite (T3 = Al); bottom, Na-exchanged Al-substituted mordenite (T3 = Si). Numbers in parentheses indicate GGA results.

mordenite is 0.15 $Å^3/SiO_2$ unit, whereas the difference in the GGA is about 0.64 $Å^3/SiO_2$ unit. Both methods lead to a higher equilibrium volume in the case of the Na-exchanged mordenite, due to the presence of the aluminum atoms and extraframework cations. The bulk modulus is slightly reduced compared to that of the pure-silica form, indicating a slight softening of the framework due to reduced symmetry. The reduction calculated in the GGA is slightly larger. The LDA method leads to better agreement with experiment (see Table 1), whereas the GGA overestimates the equilibrium volume. This confirms our conclusion reached for the denser tetrahedrally coordinated SiO_2 polytypes.[45] We note that the lattice expansion caused by the Si → Al substitution and the introduction of the Na counterions is not uniform: the cell dimensions increase along the *a* axis, remain essentially unchanged along the *c* axis, and are even slightly reduced along the *b* axis. This is clearly a consequence of the distribution of the Al sites over the framework: the T1 and T2 sites located along that part of the 12-membered ring extending in the *b* direction are occupied by Si only, while the sites situated on the sides of the ring parallel to the *a* direction are 50/50 occupied by Si and Al. Hence, a stretching of some T4−O bonds will dilate the lattice along the *a* direction. The same applies to the substitution on the T3 sites in the side pockets (cf. Figure 1).

The optimized fractional coordinates calculated in both LDA and GGA are compiled in Table 4. Due to the reduced overall symmetry, the four types of inequivalent tetrahedral sites are now split into eight types. Compared to pure siliceous mordenite, the arrangement of the tetrahedral (T, Si, or Al) and oxygen atoms is significantly changed due to the presence of eight aluminum atoms. In the following, we discuss in detail the geometry of the tetrahedral sites. Figures 4−7 summarize the information on the T−O bond lengths, the intertetrahedral bond angles, and the intratetrahedral O−T−O angles. Calculated deformation parameters may be found in Table IIS.

B. Structure of Tetrahedral Sites. *1. T3 Site.* As mentioned before, four of the T3 sites and four of the T4 sites are occupied by aluminum atoms. For the Al3 site the resulting Al−O bond lengths are increased by a maximum of 0.157 Å (LDA) and 0.161 Å (GGA) due to the larger ionic radius of Al compared to Si and the resulting distances are between 1.723−1.763 Å (LDA) and 1.731−1.786 Å (GGA), respectively (see Figure 4). The neighboring Si−O bond lengths are only slightly decreased compared to the values of the pure siliceous structure. The Al3−O9−Si3 intertetrahedral angle is decreased by ∼21° (LDA), which is one of the largest deformations occurring in Al-substituted mordenite. Furthermore, there is a strong change in the O4−Al3−O9 intratetrahedral bond angle which is expanded by ∼9° to 119° and the O1−Al3−O9 angle which is decreased to 100.4°. Although the other O−Al3−O angles are only slightly increased (∼3°) compared to that of the ideal structure, this results in strong asymmetric and rocking deformations around the Al3 site (see Table IIS). This behavior can only be interpreted if the position of the sodium counterions are taken into account. The distance between the O9 atom and one of the Na1 atoms is around 2.46 Å. This is one of the smallest values for Na−O distances (compare the Na2−O distances listed in Figure 3). Therefore, a nonnegligible "ionic" interaction between the sodium and oxygen atom is responsible for this unusual behavior, resulting in an increase of the Si−O bond. From a geometrical point of view, the oxygen atom is slightly pulled out of the framework into the channel. Furthermore, it is also remarkable that the Al3−O4−Si4 angle hardly changes. The remaining four $Si3-O_4$ tetrahedra are connected to two SiO_4 and two AlO_4 units (Figure 4). The corresponding Al−O bonds are again stretched; of the corresponding intratetrahedral angles the Si3−O4−Al4 angle (which is, with 166°, already the second largest intratetrahedral angle in pure-silica mordenite) is stretched to almost 180°, whereas the Si3−O9−Al3 angle is reduced to 131.4° (LDA). Within the Si3 tetrahedron, the Si3−O bond lengths are stretched by ∼0.025 Å, except the Si3−O4 bond directed toward the neighboring Al4 site. The most significant intratetrahedral change concerns the O1−Si3−O9 angle which is decreased to 103.2°. Altogether this already demonstrates that the changes caused by the Si → Al substitution are not restricted to the tetrahedral unit on which the substitution takes place, although the tetrahedral deformation parameters are significantly smaller than for the Al4 sites.

2. T4 Site. For the Al4 site (see Figure 5) the bond lengths and angles show the same behavior, i.e., a strong increase in the Al−O bond lengths (maximum increase about 0.127 Å) and a contraction of the Si−O bond lengths connected to the Al-containing tetrahedron. For systems which are mainly dominated by covalent bonding this alternation of expansions and contrac-

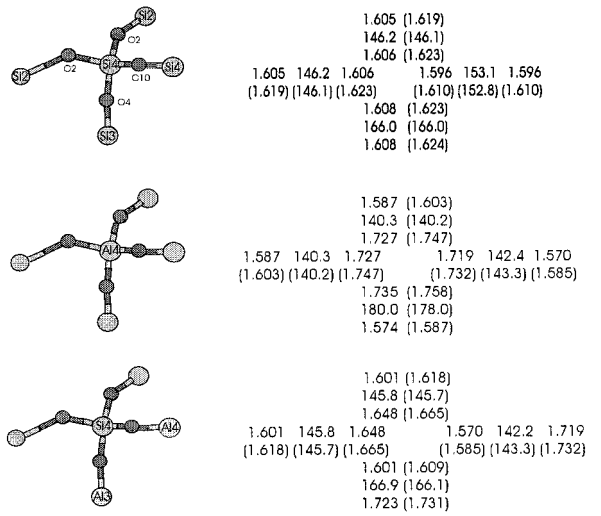

Figure 5. Bond lengths (Å) and T−O−T angles for the T4 site: top, ideal mordenite; middle, Na-exchanged Al-substituted mordenite (T4 = Al); bottom, Na-exchanged Al-substituted mordenite (T4 = Si). Numbers in parentheses indicate GGA results.

tions of bond lengths with distance from the substituting center is quite typical.[31] The Al−O bond lengths are between 1.719 and 1.735 Å (LDA) and 1.732 and 1.758 Å (GGA). On average the length of the Al−O bonds around Al4 sites is somewhat shorter (1.727 Å in the LDA, 1.746 Å in the GGA) than around the Al3 sites (1.745 Å in the LDA, 1.763 Å in the GGA). On the other hand, compared to the Al3 site the contraction of the Si−O bond is slightly larger (∼0.03 Å). This indicates a certain difference in the polarity of the AlO_4 group at the T3 and T4 sites. This is also reflected in a different distortion pattern of the Al4−O_4 tetrahedron: whereas around the Al3 site we calculate larger rocking and asymmetric deformations, on the Al4 site only the rock1 deformation indicating a tilting of the bond pointing to the protonated O site is significant. The remaining distortions are comparable or even smaller than around the nonsubstituted Si4 sites (see also below). The intertetrahedral angles again decrease by ∼11°. The Al4−O4−Si3 bond angle is stretched by ∼14 ° to 180°. Such a high value for an intertetrahedral angle is quite uncommon in silicates. As already noted, the intratetrahedral distortions around the Al4 sites are somewhat smaller than around the Al3 site. Due to this stiffness of tetrahedral bond angles, variations in the bond lengths due to Si → Al substitutions have to be accommodated by variations of the intertetrahedral angles, and this explains the large observed variations. The distortions around the remaining Si4 sites are somewhat larger concerning the Si4−O bond lengths (the largest variation of 0.042 Å occurs for the Si4−O2 bond; see Figure 5), and this leads also to rather strong symmetric as well as asymmetric deformations of the Al4−O_4 tetrahedra. The changes in the intertetrahedral angles are rather modest.

3. Sites T1 and T2. Considering the T1 and T2 sites, one has to distinguish between two different situations. Either the neighboring T atoms are as in the case for the pure-silica structure all silicon atoms, or one of the surrounding T site atoms is replaced by aluminum (see Figures 6 and 7). As a result of these different configurations the T1 and T2 sites, which have a multiplicity of 16 for the pure-silica mordenite, are therefore split in two slightly different sites, termed as Si1(1), Si1(2) and Si2(1), Si2(2), the T(1) sites having no Al neighbor. The resulting T(1,2) sites now have a multiplicity of eight. For the Si1(1) site the differences in the Si−O distances to the ideal mordenite are rather small, and some of the bonds are slightly

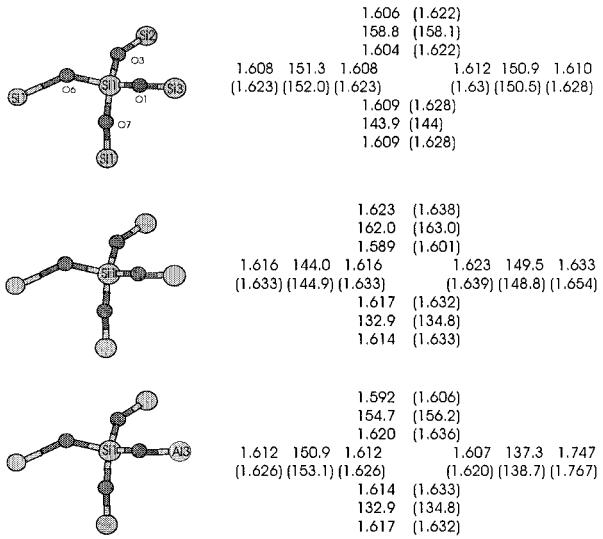

Figure 6. Bond lengths (Å) and T−O−T angles for the T1 site: top, ideal mordenite; middle, Na-exchanged Al-substituted mordenite, with no neighboring Al atom (Si1(1)); bottom, Na-exchanged Al-substituted mordenite with one neighboring Al3 atom (Si1(2)). Numbers in parentheses indicate GGA results.

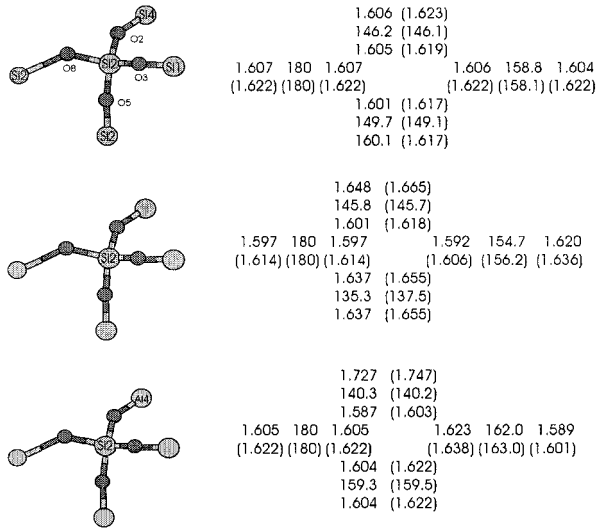

Figure 7. Bond lengths (Å) and T−O−T angles for the T2 site: top, ideal mordenite; middle, Na-exchanged Al-substituted mordenite, with no neighboring Al atom (Si2(1)); bottom, Na-exchanged Al-substituted mordenite with one neighboring Al4 atom (Si2(2)). Numbers in parentheses indicate GGA results.

increased and the others decreased (see Figure 6), leading to a significant rocking deformation (see Table IIS). A much stronger deformation occurs for the intertetrahedral angles; e.g., the Si1−O6−Si1 angle is decreased by ∼7.3°, the Si1−O7−Si1 angle by 11°. At the Si1(2) site, which has a neighboring Al3 atom, the Si1(2)−O3−Si2 angle is decreased by ∼4°, the Si1(2)−O1−Al3 angle by 13.6°. The bond lengths around Si1(2) undergo only minimal variations; even the Si1(2)−O1 bond connecting to the O1−Al3 bond is elongated only by 0.005 Å. Tetrahedral distortions are still significantly larger than in purely siliceous mordenite (cf. Tables 3 and 5).

Around the Si2(1) site (see Figure 7), one finds again only slight variations from the ideal structure. A strong decrease of about 14° occurs at the Si2−O5−Si2 bond angle. Again a quite small distance to a Na2 atom is responsible for this behavior (see also Figure 3). The Si4 → Al4 substitution close to the Si2(2) site demonstrates that distortions of the framework do

TABLE 5: O−T−O Bond Angles for Sodium-Exchanged Mordenite

	LDA	GGA		LDA	GGA		LDA	GGA		LDA	GGA
O1(1)−Si1(1)−O3(1)	114.7	114.2	O2(1)−Si2(1)−O3(1)	112.1	112.1	O1(1)−Si3−O1(1)	110.8	110.9	O1(2)−Al3−O1(2)	113.0	112.9
O1(1)−Si1(1)−O6(1)	106.1	106.2	O2(1)−Si2(1)−O5(1)	109.0	108.7	O1(1)−Si3−O4(1)	111.5	111.9	O1(2)−Al3−O4(2)	111.7	111.3
O1(1)−Si1(1)−O7	106.9	107.1	O2(1)−Si2(1)−O8(1)	111.2	111.5	O1(1)−Si3−O9	103.2	102.9	O1(2)−Al3−O9	100.4	101.0
O3(1)−Si1(1)−O6(1)	110.7	110.7	O3(1)−Si2(1)−O5(1)	107.3	107.3	O4(1)−Si3−O9	116.1	115.9	O4(2)−Al3−O9	119.0	118.9
O3(1)−Si1(1)−O7	108.6	108.8	O3(1)−Si2(1)−O8(1)	106.7	107.2	mean	109.38	109.4	mean	109.36	109.4
O6(1)−Si1(1)−O7	109.7	109.7	O5(1)−Si2(1)−O8(1)	110.4	110.0	rms	4.701	4.856	rms	6.803	6.465
mean	109.45	109.45	mean	109.45	109.46						
rms	2.817	2.604	rms	1.973	1.904	O2(2)−Si4−O2(2)	107.5	109.1	O2(1)−Al4−O2(1)	114.5	114.7
						O2(2)−Si4−O4(2)	110.3	109.4	O2(1)−Al4−O4(1)	111.8	111.0
O1(2)−Si1(2)−O3(2)	112.5	113.0	O2(2)−Si2(2)−O3(2)	114.7	113.6	O2(2)−Si4−O10	105.5	105.7	O2(1)−Al4−O10	105.6	106.0
O1(2)−Si1(2)−O6(2)	109.8	108.9	O2(2)−Si2(2)−O5(2)	103.0	103.3	O4(2)−Si4−O10	117.2	117.3	O4(1)−Al4−O10	106.9	107.6
O1(2)−Si1(2)−O7	110.9	111.1	O2(2)−Si2(2)−O8(2)	110.4	110.6	mean	109.38	109.43	mean	109.36	109.38
O3(2)−Si1(2)−O6(2)	107.3	107.8	O3(2)−Si2(2)−O5(2)	108.1	108.5	rms	4.010	3.870	rms	3.479	3.15
O3(2)−Si1(2)−O7	105.4	105.4	O3(2)−Si2(2)−O8(2)	109.3	109.9						
O6(2)−Si1(2)−O7	110.8	110.6	O5(2)−Si2(2)−O8(2)	111.2	110.8						
mean	109.45	109.46	mean	109.45	109.45						
rms	2.393	2.451	rms	3.534	3.143						

not always affect the bonds closest to the substitution site (see Figure 7): while the difference between the Si2(1)−O2−Si4 bond angle and the Si2(2)−O2−Al4 angle is only 5.5°, the Si2-(1)−O5−Si2 angle of 135.3° (which is decreased by 14.4° compared to that of the pure-silica case) increases by 24° to 159.3° due to the substitution on the T4 site. One of the reasons for this exceptionally large distortion is that the Si2−O8−Si2 angle is constrained to 180° by symmetry so that the distortions necessary to accommodate the long Al4−O2 bond cannot be distributed over a large number of degrees of freedom.

The difference between the Si1(1) and Si1(2) sites is of course also indicated by different fractional coordinates (see Table 4). Similarly the O1 to O6 and the O8 sites are split into two classes, depending on the occupation of the neighboring tetrahedral sites by Si or Al. It is remarkable that this splitting of internal parameters does not occur for the O7, O9, and O10 oxygen sites. The O9 and O10 sites occupy high-symmetry positions in the undistorted pure-silica framework. Oxygen atoms which occupy the O7 site have a rather large distance to an aluminum or sodium atom. Therefore, the influence of these atoms, which are mainly responsible for the splitting of positions, is rather small. The greater irregularity of the tetrahedral framework in Na-mordenite compared to the pure-silica case is best illustrated by considering the distribution of the T−O bond lengths and O−T−O angles. Figure 2S shows the distribution of the T−O bond lengths in the case for ideal and Al-substituted mordenite. Within the LDA approximation the Si−O bond lengths calculated for the purely siliceous mordenite range between 1.596 and 1.613 Å, with three main peaks between 1.604 and 1.609 Å. For the Al-substituted structure there is a significant splitting of the T−O bond lengths over a much wider range. The Al−O bond distances are in a range from 1.718 to 1.763 Å (LDA) and 1.732 to 1.786 Å (GGA). For the Si−O distances in the Al-substituted structure the differences between the smallest and largest distances are now 0.056 Å (LDA) and 0.055 Å (GGA). For the intratetrahedral O−T−O bond angles (see Figure 3S) the range for the ideal structure is 108−111° with a maximum at 109.02°, which is quite similar to the ideal tetrahedral angle of 109.43°. Again a much wider distribution is found with angles varying from 100° to 119° (LDA and GGA), but retaining the ideal tetrahedral angle on average.

V. Structure of Protonated Mordenite

Considering the four distinct T sites in the mordenite structure, there are 14 possibilities to protonate a certain oxygen atom neighboring a tetrahedral aluminum atom. However, any chemical reaction (adsorption, isomerization, etc.) involving larger molecules could only occur in the main channel due to the geometry of the zeolite. Therefore, only those O−H bonds which are pointing into the main channel are of interest in the present study. This reduces the number of possible Brønsted acid sites which have to be analyzed to seven. Possible protonation sites are O3 and O7 next to Al1; O2, O3, and O5 next to Al2; and O2 and O10 next to Al4. The location of the selected acid sites is shown in Figure 8. Note that only the last two sites have been included in our study of Na-exchanged mordenite. The OH groups attached to the O3, O7, and O10 sites are heading toward the center of the 12 MR (membered ring), whereas those located at the O5 sites point toward the center of the 8 MR. Alberti[53] has suggested on the basis of a comparison of crystal structure refinements and data from infrared spectroscopy that about 2/3 of the OH groups present at Si/Al ratios ranging

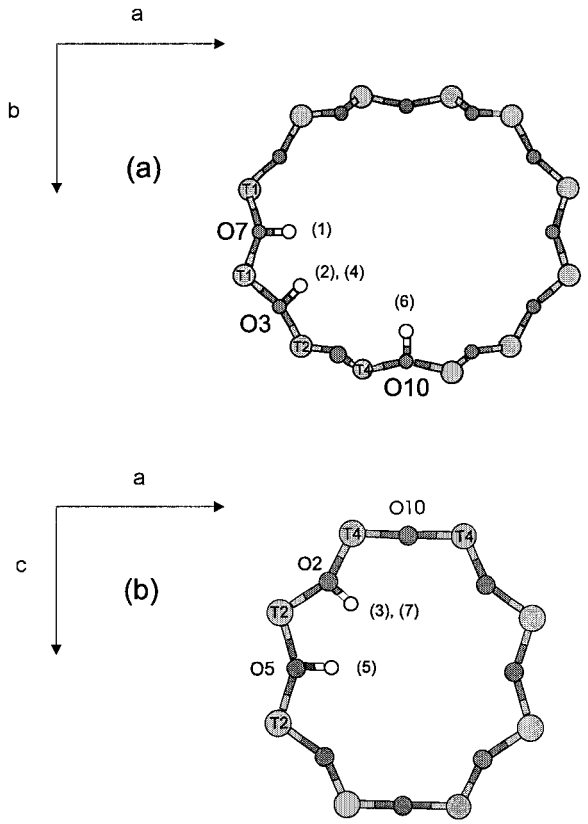

Figure 8. Location of the acid sites in mordenite considered in the present study: (a) sites 1 and 2 close to the T1, site 4 at T2, and site 6 at T4 in the twelve-membered ring; (b) site 7 at T4 and sites 3 and 5 at T2 in the eight-membered ring (side pocket).

TABLE 6: O−T−O Bond Angles for Protonated Mordenite

	LDA	GGA		LDA	GGA
Acid Site Al1−O7					
O1−Al1−O3	118.7	120.1	O3−Al1−O6	115.3	116.1
O1−Al1−O6	114.2	113.1	O3−Al1−O7(H)	95.4	93.1
O1−Al1−O7(H)	106.1	105.9	O6−Al1−O7(H)	103.4	104.2
Acid Site Al1−O3					
O1−Al1−O3(H)	105.5	107.0	O3(H)-Al1−O6	104.7	105.4
O1−Al1−O6	116.4	114.6	O3(H)-Al1−O7	93.9	91.6
O1−Al1−O7	115.0	116.0	O6−Al1−O7	117.1	118.0
Acid Site Al2−O2					
O2(H)-Al2−O3	107.2	105.4	O3−Al2−O5	115.0	116.8
O2(H)-Al2−O5	97.5	96.1	O3−Al2−O8	114.7	113.7
O2(H)-Al2−O8	101.4	104.2	O5−Al2−O8	117.7	117.1
Acid Site Al2−O3					
O2−Al2−O3(H)	96.3	95.6	O3(H)-Al2−O5	102.2	106.4
O2−Al2−O5	115.3	114.9	O3(H)-Al2−O8	106.2	103.0
O2−Al2−O8	117.8	119.1	O5−Al2−O8	115.1	114.1
Acid Site Al2−O5					
O2−Al2−O3	118.4	118.5	O3−Al2−O5(H)	107.0	108.0
O2−Al2−O5(H)	94.1	90.0	O3−Al2−O8	113.9	112.7
O2−Al2−O8	113.1	114.7	O5(H)-Al2−O8	107.6	109.2
Acid Site Al4−O10					
O2−Al4−O2	113.1	116.6	O2−Al4−O10(H)	98.5	95.6
O2−Al4−O4	117.5	115.8	O4−Al4−O10(H)	107.5	107.7
Acid Site Al4−O2					
O2−Al4−O2(H)	105.9	107.9	O2−Al4−O10	117.4	116.1
O2−Al4−O4	113.0	113.1	O2(H)-Al4−O10	96.3	92.6
O2(H)-Al4−O4	105.6	105.6	O4−Al4−O10	115.9	118.1

between 4 and 6 belong to sites in the 12 MR and 8 MR (and are accessible to large molecules such as benzene), while the remaining 1/3 are located in the small 8 MR and accessible only to small molecules. In our study we have considered first only a single H atom per elementary cell; this allows the properties of individual acid sites to be characterized. Again both methods (LDA and GGA) have been used and a full structural optimization has been performed for all seven cases. At this low Al/Si ratio, there are only minimal changes in the lattice parameters compared to those of the pure-silica case, but the substitution breaks the point group symmetry of the cell. VASP performs a symmetry analysis of the starting structure and relaxes the lattice under the constraint of this reduced symmetry. For each acid site, the starting structure has been chosen in such a way that, using the experimental lattice constants,[22] the Al−O−H angle is equal to the Si−O−H angle. Furthermore, the hydrogen atom is placed in the plane formed by the silicon, oxygen, and aluminum atoms. Initially, the O−H distance was set to 1 Å. In the following, we discuss in detail the geometry of the individual acid sites.

A. Acid Groups Close to the T4 Sites. Only for the T4 site one can directly compare the results for structural relaxations concerning all three different cases of Al-free, Na-exchanged, and protonated structures. The most significant difference occurs at the Al−O(H) bond (see Figure 9). The Al4−O2(H) bond length is increased to 1.85 Å (LDA) and 1.87 Å (GGA), respectively (in the ideal structure this value is 1.606 Å (LDA) and 1.623 Å (GGA), and for the Na-exchanged it is 1.727 Å (LDA) and 1.747 Å (GGA), respectively). The other three Al−O distances in the tetrahedron change much less (by 0.07−0.09 Å) compared to those of pure-silica mordenite; compared to those of the Na-exchanged structure, these distances are shorter. These strong differences in the bond lengths also lead to strong deviations of the AlO_4 cluster from tetrahedral symmetry. The calculated O−T−O angles are listed in Table 6. Tetrahedral deformation parameters are compiled in Table IIIS. For the

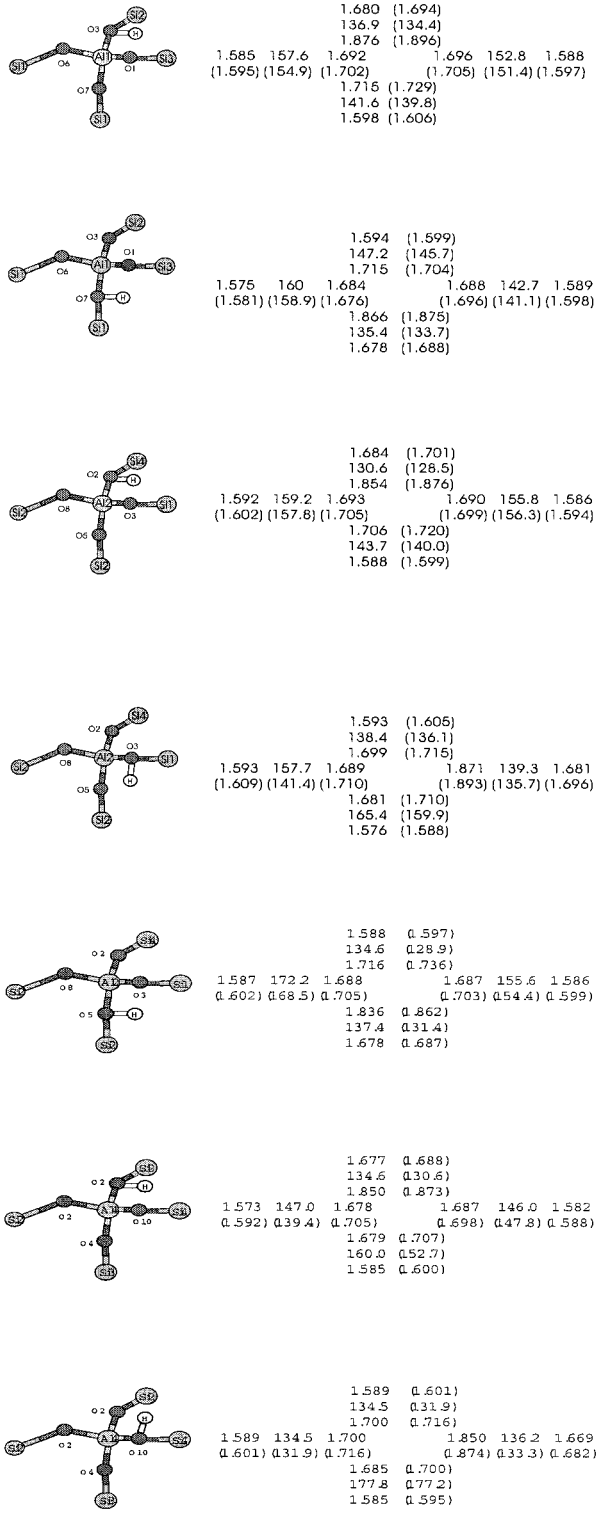

Figure 9. Bond lengths (Å) and T−O−T angles for seven distinct acid sites. Numbers in parentheses indicate GGA results.

Al4−O2 acid site this distortion is characterized by strong symmetric deformations, resulting from a strong decrease of all angles which involve the Al4−O2(H) bond (the O2−Al4−O10 angle is even decreased to 96.3°). This distortion is even stronger in the GGA. The Al4−O2(H)−Si2 angle is again reduced by 11.6° to 134.6° (LDA). This behavior is quite similar for all protonated structures: the intertetrahedral angle which describes the bending of the corner-sharing tetrahedra has its lowest value compared to those of the ideal and Na-exchanged phases at the protonated O site. Within the GGA method this

reduction is even larger (~15.5° to 130.6°). Again, the amplitude of the changes decreases with increasing distance from the site of perturbation due to substitution and protonation. With the exception of the Si2−O2(H) bond length, which is expanded by 0.07 Å (LDA and GGA) all other neighboring Si−O distances are decreased, therefore showing the same behavior as in the case for Na-exchanged mordenite. Another interesting feature of the T4 site is that if the H atom is attached to the O2 atom, the Al4−O4−Si3 angle is changed only very slightly within the LDA by ~6°, whereas within the GGA this angle is decreased by ~13° compared to the values in the pure-silica phase. This decrease of the Al4−O4−Si3 angle is accompanied by a stretching of the remaining intertetrahedral angles. Note that in Na-mordenite this angle is nearly 180°, but only 166° in the pure-silica case. Hence, in this case protonation of the O2 site even reduces the strain on the intertetrahedral bond.

Comparing LDA and GGA results, there is a clear trend that by using gradient-corrected functionals the distortions of the AlO_4 (H) tetrahedra are larger than by using the local-density approximation. The fact that stronger distortions result from the GGA calculations is remarkable. In our studies of silica polymorphs[45] and also in the work described in the previous sections, we have found that at fixed volume LDA and GGA lead to almost identical structural predictions. However, we have to remember that these studies refer to homogeneous structural changes distributed over the entire framework, whereas here we study a very local perturbation. The GGA predicts a more pronounced increase of the Al−O(H) bond length, and this leads immediately to stronger distortions of the surrounding framework. Note that for both methods the same equilibrium volumes have been used. The geometrical differences are much smaller for the pure-silica and Na-exchanged mordenite, because LDA and GGA leads to nearly identical results for the same volume. If the H atom is attached to the O10 site instead of to the O2 atom, the local distortions of the AlO_4 tetrahedra and of their connections to the remaining framework follow a quite different pattern: Although the Al−O bonds to the nonprotonated sites are slightly longer, the distortion of the tetrahedral symmetry is distinctly weaker. The intertetrahedral angles, however, show pronounced changes relative to those of the pure-silica case: in particular, the Al4−O4−Si3 angle is stretched to nearly 180°, whereas the other angles are strongly reduced. Note that a similar change was also observed in Na-mordenite.

B. Acid Groups Close to the T2 Sites. For the Al2 site three different oxygen atoms can be protonated, i.e., O2, O3, and O5 (see Figure 9). Again a strong expansion of the Al−O(H) and Si−O(H) distances occurs, with a correlated decrease of the intertetrahedral angles. The distortions of the AlO_4 tetrahedron, however, are quite different depending on the choice of the protonation site: In the Al2−O2−H case, the distortion is predominantly symmetric (cf. Table IIIS), for the Al2−O3−H rocking deformations are dominant and the same also applies to the Al2−O5−H acid site. A remarkable difference between the three protonated oxygen atoms can be seen at the Al2−O8−Si2 angle. In the ideal structure this angle is 180° (see Table 3). For the Al2−O5(H) case this angle is only slightly decreased, 172° (LDA). For the other two cases this angle is much smaller; for O2(H) it is 159.2°, and for O3(H) it is 157.7°. This behavior is due to topological differences of the oxygen atoms. The O3 atom belongs only to the main 12 MR ring, the O5 atom is building up the side pockets (8 MR) (see also Figure 8), and the O2 atom belongs to both 12- and 8-membered rings. Therefore, the greatest change occurs for the O3 site. Within the GGA this angle is even reduced to 141.4°.

C. Acid Groups Close to the T1 Sites. The strongest distortions within the AlO_4 tetrahedra occur if one of the O sites close to a T1 site is protonated (O3 or O7). In both cases we find strong symmetric, asymmetric, and rocking deformations (see Table IIIS). On the other hand, the flexibility of the intratetrahedral bonds leads to smaller strains on the intertetrahedral connections. Except for the Al1−O3(H)−Si2 angle, which is reduced by about 22° compared to that of the purely siliceous case, all other intertetrahedral angles undergo only modest changes.

D. Long-Range Distortions of the Framework. So far analysis has concentrated on local distortions around the protonation sites. It is clear, however, that distortions as large as the reduction of the intertetrahedral T2−O8−T2 angle from the value of 180° characteristic for the purely siliceous structure to 141.4° if the O3 atom at the other side of the Al2 atom is protonated will also affect the remaining framework. The problem is that such distortions are difficult to grasp. As an illustrative example, we describe here the variation of the straight T2−O8−T2 bonds which are a characteristic feature of the centrosymmetric idealized mordenite structure and which exist also in our version of Na-mordenite with a 50/50 Al/Si ratio on the T3 and T4 sites. Altogether, there are eight such straight T2−O8−T2 bonds per unit cell (see Figure 1; note that pairs of bonds are superposed in a projection along the *c* direction). Figure 12 displays the calculated values for these bond angles for our seven different protonated structures. For certain acid sites, protonation occurs on one of the TO_4 tetrahedra forming such a straight bond in the idealized structure. The corresponding angles are highlighted in Figure 12; they usually show the strongest reduction (by nearly 40° for the Al2−O3−H site, calculated in the GGA). However, comparable distortions occur also if one of the more distant oxygen sites is protonated, as demonstrated by the Al4−O10−H site.

We have included these results here, because they demonstrate the particular flexibility of zeolite framework, which allows quite large changes in the bond lengths due to protonation to be accommodated with relatively modest distortions of the intertetrahedral angles. Optimizations of cluster models for acid sites often lead to intertetrahedral angles ranging between about 110° and 130°, i.e., considerably smaller than any of the T−O−T (including Al−O−Si) angles found in this study.[31,32] The reason is that the constraints applied to the outer boundaries of the cluster are rather inappropriate to mimic a flexible environment.

E. Configuration of the Hydroxyl Groups. Although we have recorded quite different intertetrahedral distortions and changes in the intertetrahedral networks, depending on the locations of the acidic proton, the variations in the geometry of the Al−O(H)−Si groups themselves are surprisingly small. For all acid sites, the length of the O−H bond differs only very slightly from the initial value of 1 Å. In the LDA the O−H bond lengths vary between 0.993 and 0.999 Å; the GGA leads to slightly shorter O−H bonds. This is remarkable since it contrasts the general tendency toward increased bond lengths when gradient corrections are added to the LDA functional. Here we find that the GGA leads to a more pronounced increase of the Al−O(H) and Si−O(H) distances than observed for the remaining Si−O bond lengths. Hence, the GGA changes the polarity of the Al−O−H group, resulting in a stronger binding within the hydroxyl group.

Initially, the O−H groups are located within the plane of the twelve- or eight-membered ring, respectively, and form equal Al−O−H and Si−O−H angles. The location within the plane is maintained to good accuracy; the largest out-of-plane angle

TABLE 7: Selected Geometrical Parameters (O−H Bond Lengths (Å), Si−O−H and Al−O−H Angles (deg)) of the Optimized Structures for Seven Brønsted Acid Sites in Mordenite[a]

	LDA			GGA		
	O−H	Si−O−H	Al−O−H	O−H	Si−O−H	Al−O−H
			(a) Al/Si = 1/47			
(1) Al1−O7−H	0.9972	117.3	107.3	0.9924	117.6	108.7
(2) Al1−O3−H	0.9981	117.5	104.1	0.9967	118.6	106.9
(3) Al2−O2−H	0.9935	116.7	112.4	0.9914	118.1	112.9
(4) Al2−O3−H	0.9934	114.4	106.3	0.9939	115.5	108.4
(5) Al2−O5−H	0.9961	115.3	107.3	0.9946	120.9	107.6
(6) Al4−O10−H	0.9953	116.6	107.2	0.9932	115.7	111.0
(7) Al4−O2−H	0.9997	117.6	107.6	0.9935	120.0	109.3
			(b) Al/Si = 1/11			
(1) Al1−O7−H	0.9985	121.0	103.2	0.9957	121.3	103.4
(2) Al1−O3−H	1.006	119	95.2	1.000	117.7	100.3
(3) Al2−O2−H	0.9944	116.2	107.3	0.9903	117.2	114.2
(4) Al2−O3−H	1.004	121.2	98.8	0.9959	118.5	107.1
(5) Al2−O5−H	0.9971	118.9	106.1	0.9945	120.7	109.8
(6) Al4−O10−H	0.9942	116.1	107.5	0.9917	117.2	108.5
(7) Al4−O2−H	0.9952	116.6	106.2	0.9942	117.6	108.5

[a] Left part: LDA results. Right part: GGA results. Part a lists the results calculated for a single acid site per cell, part b those for four acid sites per cell.

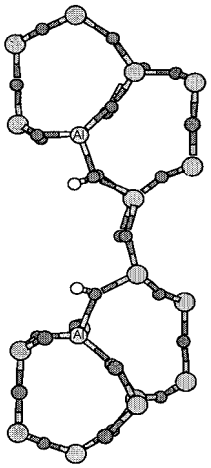

Figure 10. Neighboring of two acid sites for Al2−O3H protonation.

is about 3°. After the relaxation, the Al−O−H angle is always smaller than the Si−O−H angle; the largest difference is found at the Al1−O3−H site with about 13°.

F. Increased Al/Si Ratio. Interaction between Acid Sites. To study the influence of a higher concentration of acid sites, we have studied protonated mordenite with an Al/Si ratio of 1/11. We have studied again the same seven types of acid sites, but now four out of sixteen T1 or T2 sites or four out of eight T4 sites are occupied by Al. For each of these four Al sites, the hydrogen atom was attached to topologically identical oxygen atoms. If one compares directly the distances and angles of $HAlSi_{47}O_{96}$ and $H_4Al_4Si_{44}O_{96}$, the differences in the local structure of the acid site turn out to be very small. The differences in the bond lengths are smaller than 0.02 Å; the differences in the angles are about 1.5°. The exception is the Al2−O3(H) site, where the structural difference is much larger. In this case the substitution of four Si atoms leads to a structure where neighboring acid sites are separated only by a short Si−O−Si bridge (see Figure 10). As a result the value for the Si1−O7−Si1 angle, which is ∼144° in the pure-silica phase (see Table 3) and ∼147° for one acid site per cell, increases to 154° for the $H_4Al_4Si_{44}O_{96}$ phase.

The increased Al/Si ratio and the higher degree of protonation have only a very small influence on the O−H bond length; some bonds are elongated, and others shrink. On the other hand, the higher Al/Si ratio always leads to a stronger asymmetry of the Al−O−H and Si−O−H angles. For instance for the Al2−O3−H site, the Si−O−H angle is expanded to 121.2° accompanied by a reduction of the Al−O−H angle to 98.8°. Furthermore, the O−H distances are slightly increased to 1.004 Å. Again this is caused by the interaction between the neighboring two acid sites (see Figure 10).

VI. Energetics of Acid Sites and O−H Stretching Frequencies

After discussion of the structural properties of protonated mordenite, the next step is a detailed analysis of the relative stability of the protonation sites. From a catalytic point of view not only the energetics but especially the strength (acidity) is of interest. A frequently used measure of acidity is the O−H stretching frequencies, which characterize not only the Brønsted acid sites but also the interaction with adsorbate molecules in zeolites.

A. Relative Energies of Acid Sites. The Al1−O3 site is found to have the lowest energy within both methods (LDA and GGA) (see Table 8). Additionally, within both LDA and GGA the Al4−O10 acid site has the highest energy. The orders of stability are slightly different: LDA, Al1−O3 < Al2−O2 < Al2−O3 < Al4−O2 < Al2−O5 < Al1−O7 < Al4−O10; GGA, Al1−O3 < Al2−O3 < Al2−O2 < Al2−O5 < Al4−O2 < Al1−O7 < Al4−O10. The energy difference between the most stable and least stable positions is 0.272 eV (LDA) and 0.29 eV (GGA), respectively.

There exists a connection between local structure and protonation energy. For the Al1−O3 and Al2−O3 protonation sites the Si−O−Si angles in the purely siliceous structure are around 158°. The sites with larger intertetrahedral angles have a higher capacity to accommodate distortions arising from Si → Al substitution and protonation. This flexibility is decreased for sites with more acute Si−O−Si angles (between 143° and 149°) for which protonation is therefore less favorable. However, the situation is not that simple, as demonstrated by the Al4−O10 site, which is least favorable, but also has a high value for this angle (153°). Additionally one has to take into account that there are acid sites where the substitution site is connected to the rest of the framework by an intertetrahedral angle of nearly 180°. This is exactly the case for the Al4−O10 site (Al4−O4−Si3) (see Figure 5). This unusually high value indicates that there is a large local strain on this bond, leading to an increased

TABLE 8: Relative Energies ΔE (eV), Anharmonic (ω_{01}, ω_{anh}) and Harmonic (ω_e, ω_{harm}) O−H Stretching Frequencies (cm^{-1}), and Anharmonicity Parameter ($\omega_e\chi_e$) for Seven Different Acid Sites in Mordenite[a]

			quantum			classical		
position		ΔE	ω_{01}	ω_e	$\omega_e\chi_e$	ω_{anh}	ω_{harm}	$\Delta\omega$
(1) Al1−O7	LDA	0.127	3539	3712	86.7	3519	3755	236
	GGA	0.230	3601	3785	91.8	3532	3814	282
(2) Al1−O3	LDA	0.0	3521	3710	85.2	3493	3690	197
	GGA	0.0	3552	3739	93.3	3534	3774	240
(3) Al2−O2	LDA	0.016	3567	3738	85.4	3549	3784	235
	GGA	0.057	3597	3777	90.2	3595	3826	231
(4) Al2−O3	LDA	0.084	3531	3703	86.4	3507	3744	237
	GGA	0.028	3595	3779	92.3	3582	3806	224
(5) Al2−O5	LDA	0.108	3515	3686	85.6	3499	3730	231
	GGA	0.097	3587	3770	91.7	3579	3809	230
(6) Al4−O10	LDA	0.272	3556	3728	86.4	3532	3770	238
	GGA	0.290	3618	3797	89.5	3604	3832	228
(7) Al4−O2	LDA	0.102	3534	3707	86.7	3528	3751	223
	GGA	0.175	3606	3790	92.0	3595	3823	228
av	LDA		3537	3712	86.0	3518	3746	228
	GGA		3593	3776	91.3	3574	3812	238
rms	LDA		45.2	41.4	1.5	48.6	74.3	35.9
	GGA		50.9	46.1	3.1	72.3	47.0	49.4
exptl			3616[b]		82[c]		3616[b]	

[a] Calculated in LDA and GGA. Left part: quantum-mechanically calculated frequencies (by solving numerically the Schrödinger equation). Right part: classical calculation via Morse fits. ΔE is the relative energy to the most stable acid site (i.e., Al1−O3). [b] Reference 54. [c] Referece 60.

protonation energy. The correlation with the intratetrahedral distortions on the other hand is weak: the energetically most favorable acid site (Al1−O3) shows strong symmetric, asymmetric, and rocking deformations from the ideal geometry; the least favorable one (Al4−O10) shows a large symmetric deformation (but weaker asymmetric or rocking distortions). The correlation between a larger intertetrahedral angle at the protonation site with a lower energy agrees with similar results derived from cluster studies of acid sites.[31−33] This correlation has been attributed to the covalent nature of the O−H bond, an increasing T−O−T angle favoring sp over sp^2 hybridization of the oxygen states and the increased OH angle favoring the formation of an O−H bond.

B. Vibrational Properties of the Hydroxyl Groups. The O−H vibrational frequencies have been calculated using two different approaches. First, the potential energy as a function of the O−H bond length has been fitted for small deviations ranging within ±0.05 Å from the equilibrium bond length, using a third-order polynomial approximation to the Morse potential. The frequencies are derived from the first numerical derivatives. In the second approach, the potential energy curves are fitted by a sixth-order polynomial (for further details see section II) and the vibrational frequencies are calculated by integrating the one-dimensional Schrödinger equation. Note that a relatively large interval of bond length stretchings (from −0.2 to +0.3 Å) is necessary to cover at least three vibrational levels. The calculated frequencies are summarized in Table 8. Anharmonic stretching frequencies (ω_{01}), derived from a series of static single-point total-energy calculations and solving numerically the one-dimensional Schrödinger equation, fall into an interval ranging from 3515 to 3567 cm^{-1} (LDA) and 3552 to 3618 cm^{-1} (GGA), respectively. By using Morse fits, we calculated frequencies (ω_{anh}) ranging from 3493 to 3549 cm^{-1} (LDA) and 3532 to 3604 cm^{-1} (GGA), respectively. The first conclusion is that the result of the quantum mechanical calculation differs from the classical result by only about 20 cm^{-1}. Hence, a classical treatment is quite adequate. Comparing the two different exchange correlation functionals, one notes that the GGA gives for each acid site higher frequencies in both harmonic and anharmonic approximations. The higher frequencies calculated in the GGA are a direct consequence of the shorter O−H bond length as discussed in the previous section. The values for the frequencies reported so far are based on a rigid framework, allowing no relaxation. To study possible effects of the structural relaxation, we recalculated the potential energy curves, allowing the whole framework to relax. Only for the Al1−O7, Al1−O3, and Al2−O5 acid site we obtained measurable differences in the potential energy curves. For these three sites, the recalculated stretching frequencies are given in Table 9. While all harmonic frequencies are reduced by the lattice relaxation, the anharmonic frequencies increase for the Al1−O7 site, decrease for the Al1−O3 site, and are almost unchanged for the Al2−O5 site. For all sites we note a reduction of the anharmonicity. Altogether these results confirm that the O−H stretching frequencies are essentially decoupled from the degrees of freedom of the framework.

TABLE 9: Anharmonic and Harmonic Frequencies (cm^{-1}) Calculated from the Morse Fits to the Potential Energy Curves Allowing a Relaxation of the Lattice[a]

position		ω_{anh}	ω_{harm}	$\Delta\omega$
Al1−O7	GGA	3583 (3532)	3772 (3814)	189 (282)
Al1−O3	GGA	3510 (3534)	3711 (3774)	201 (240)
Al2−O5	GGA	3586 (3579)	3776 (3809)	190 (230)

[a] Values in parentheses represent the results calculated for a rigid framework.

A typical FT-IR spectrum[54−58] of bare H-mordenite shows two adsorption bands at 3750 cm^{-1} and at about 3616 cm^{-1}. The weaker band at 3750 cm^{-1} is assigned to the OH modes of the terminal silanol group located at either the external surface or framework defects. The stronger band at about 3616 cm^{-1} is assigned to the OH mode of the hydroxyl groups bridged in the form of Al−OH−Si which are located inside the channels and attributed to be the origin of the Brønsted acidity. The slightly asymmetric band at ∼3616 cm^{-1} has been deconvoluted into two bands at ∼3609−3617 and 3585−3590 cm^{-1} contributing in a ratio of about 2/1 to the IR spectrum. The band at ∼3609−3617 cm^{-1} has been assigned to hydroxyl groups in the 12 MR, the weaker low-frequency band to acid sites in the smaller cavities (8 MR or side pockets).[54−58] Studies of alkane

adsorption[59] in mordenite suggest the low-frequency band should be assigned to hydroxyl groups in side pockets alone. However, one has to emphasize that, considering the small difference between the high-frequency (HF) and low-frequency (LF) bands ($\sim$25 cm^{-1}, i.e., about the same as the line widths themselves), structure−frequency correlations are expected to be weak. The experimental value of 3609−3617 cm^{-1} for the HF component of O−H stretching frequencies (this is the proper reference for the acid sites considered in our study) is in very good agreement with the average frequencies calculated within the GGA: 3593 $\pm$ 50 cm^{-1} (quantum approach), 3574 $\pm$ 72 cm^{-1} (classical calculation). The LDA leads to frequencies that are lower by about 60 cm^{-1}. The values for the anharmonicity constants ($\omega_e\chi_e$) are in good agreement with the experimental values obtained for H-mordenite (82.5 $\pm$ 1 cm^{-1}) by Garrone et al.[60]

C. Correlation between Acid Site Geometry and O−H Stretching Frequencies. To explore the correlation between O−H stretching frequencies (and hence acidity) and the local geometry of the acid sites, we have plotted in Figure 11 the calculated frequencies against the O−H bond length, the intertetrahedral Al−O−Si bond angle at the acid site, and the Al−O−H angle. Although within this relatively narrow range the O−H vibrational frequencies show considerable scatter, we can see that the frequencies decrease with (a) increasing O−H bond length, (b) increasing Al−O−Si angle, and (c) decreasing Al−O−H angle. The correlation between an increased O−H distance and a lower IR frequency is the expected result, an increased bond length reflecting a weaker bonding. The increased bond length also correlates reasonably well with a decreased Al−O−H bond angle (cf. Table 7): a small angle reflects a larger local strain on the bonding, leading to a somewhat looser O−H bond. The correlation between an increasing Al−O−Si angle and a decreasing O−H stretching frequency leads back to energetic consideration: In section VI.A we have pointed out that sites with larger intertetrahedral angles have a higher capacity to act as substitution/protonation sites; here we find a lower strain on the surrounding framework also results in a lower O−H frequency. In accordance with these arguments we also found a certain correlation between the energetics and the vibrational properties, at least in the GGA. Both quantum and classical calculations lead to the lowest IR frequencies for the energetically most favorable site (Al1−O3: $\omega_{quantum} = 3552$ cm^{-1}, $\omega_{classical} = 3534$ cm^{-1}) and to the highest frequencies for the least favorable site (Al4−O10: $\omega_{quantum} = 3628$ cm^{-1}, $\omega_{classical} = 3604$ cm^{-1}). However, the ordering of the frequencies does not follow strictly the energetic preference; in the LDA the correlation is less clear. This should not be considered as too surprising, as the O−H stretching frequency measures the curvature of the potential energy surface rather than the depth of the attractive minimum.

We should certainly not forget to emphasize that the correlations discussed here are rather weak—and this is to be expected to be so because the easily accessible acid sites we have selected for our study share common characteristics, all being located at the boundaries of the large cavities in the mordenite framework.

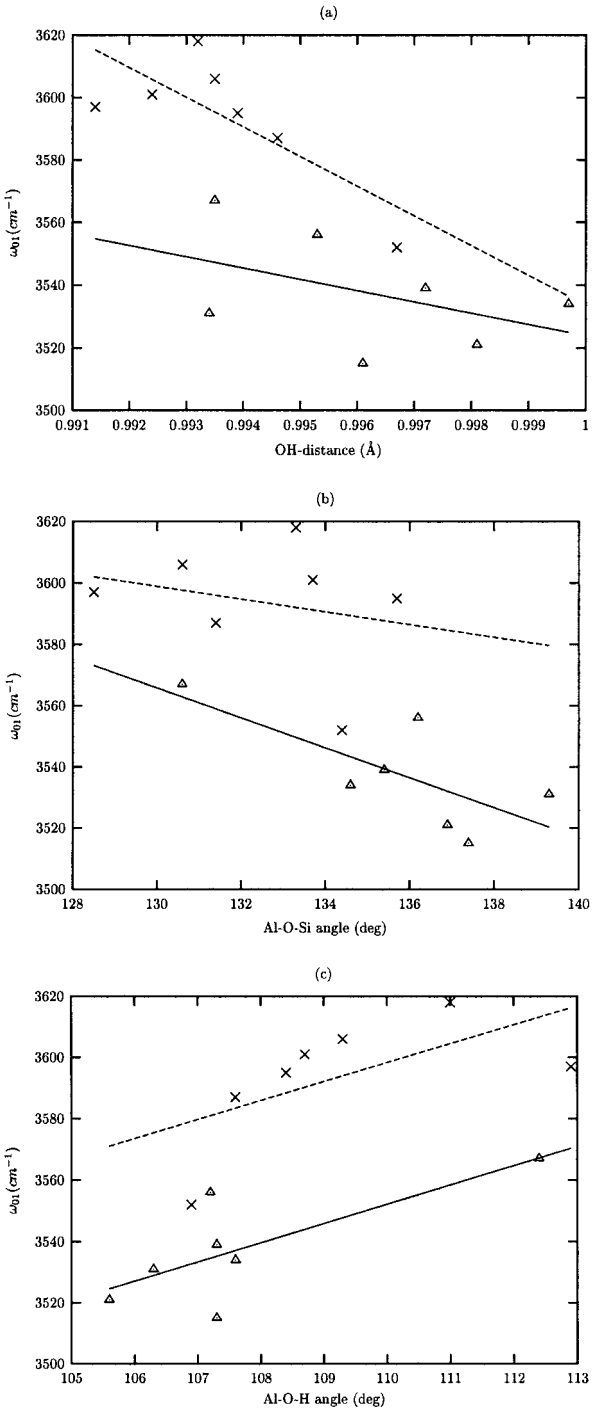

Figure 11. Correlation of the (a) O−H distance and (b) Al−O−Si and (c) Al−O−H angles with the anharmonic O−H vibrational frequencies. Triangles and solid lines indicate LDA results, crosses and broken lines GGA results. The lines represent least-squares fits to visualize the general trends.

VII. Discussion and Conclusions

In this paper we have presented detailed local-density-functional studies of the structural properties of mordenite, a zeolite compound with important applications in catalysis. Three different forms of mordenite have been studied: (i) the purely siliceous framework with composition $Si_{48}O_{96}$, (ii) an aluminosilicate form with an Al/Si ratio of 1/5 and containing Na counterions (composition $Na_8Al_8Si_{40}O_{96}$) which is quite close to natural Na-exchanged and dehydrated mordenite, and (iii) protonated mordenite with Al/Si ratios of 1/47 and 1/11 and different locations of the protonated oxygen site. For the pure-silica and Na-exchanged mordenites a full structural optimization (lattice constants and internal parameters) has been performed; for the protonated forms structural optimizations at fixed cell volumes and detailed studies of the vibrational dynamics of the hydroxyl groups at the acid sites are presented.

For the pure-silica form we find very good agreement of the lattice constants and the internal parameters with experiment if

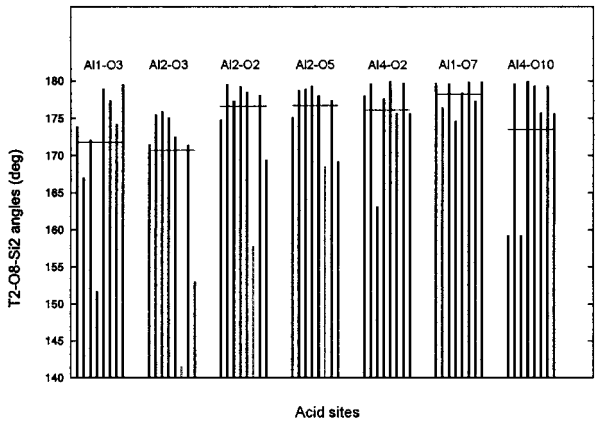

Figure 12. Variation of the straight T2−O8−T2 angles (=180° in the pure-silica and Na-exchanged cases) due to protonation. The dashed bars highlight those angles connecting directly to a protonated TO_4 tetrahedron. The horizontal lines indicate the mean values. Only GGA results are shown.

the LDA is used; the GGA leads to a slight overestimate of the cell volume, but to almost identical internal parameters. The optimized pure-silica mordenite structure consists of a very regular network of SiO_4 tetrahedra, with deviations from the ideal tetrahedral geometry which are much smaller than estimated by most diffraction experiments. This agrees with the experimental observation of an increased tetrahedral perfection at a reduced Al/Si ratio and at decreased water content, and with previous studies predicting the lowest energies for the structures with the smallest fluctuations in Si−O bond lengths and intratetrahedral angles.

The substitution of Si by Al leads to a strong but localized deformation of the tetrahedral network. All Al−O bonds within the AlO_4 tetrahedra are expanded, and the intertetrahedral angles are reduced. To compensate for the local expansion around the Al sites, the Si−O bonds connecting to the neighboring SiO_4 tetrahedra are slightly compressed. In our study we have investigated a configuration with an Al/Si ratio of 1/1 on the tetrahedral sites T3 and T4 forming the small four-membered rings in the structure, and no Al on the T1 and T2 sites located at the boundaries of the main cavities, leading to an overall Al/Si ratio of 1/5. The eight Na counterions have been distributed over two different sites; four ions are placed into the center of the eight-membered ring and four into the center of the side pockets. After structural relaxation, the first group of Na ions remain in their high-symmetry position, whereas the second class of Na ions drift to an off-center position closer to the framework atoms. The close approach of the counterions to the framework is found to induce additional distortions of the local geometry. We also show that the T1 and T2 positions occupied by silicon atoms only split into two classes, depending on the occupation of a neighboring T site by Al or not. In all cases the lattice distortion around the substitution site does not extend beyond the second shell of neighbors.

In the study of protonated mordenite we concentrated on those possible protonation sites where the hydroxyl group points into the main channel and is hence accessible to contacts with even moderately large atoms. This restricts the number of possible acid sites from fourteen to seven. For all seven sites a full structural optimization has been performed. At the very low Al/Si ratio of 1/47 a change of the lattice constants induced by the Si/Al substitution on protonation can be neglected, but the symmetry reduction resulting from the substitution has been taken into account. Compared to Na-mordenite, the protonation induces a further increase of the Al−OH bond length, accompanied by a decrease of the neighboring Si−O distances and an increase of the Si−OH bond length. As a consequence of the larger changes in the bond lengths induced by Si/Al substitution and protonation, the structural distortions are not as strictly localized as in Na-mordenite. We have found quite long-ranged deformations of the straight T−O−T bonds characteristic of the mordenite structure. This flexibility of the zeolitic framework allows the angular distortions to be distributed over a larger area, leading to smaller distortions of the local Al−O−Si angles than estimated on the basis of cluster calculations. While for the phases not containing acid sites LDA and GGA lead to almost identical structures at fixed volume, the gradient corrections are quite important for the structural characterizations of the acid sites, leading to a pronounced increase of the Al−OH bond lengths by 0.02 Å on average, whereas the Si−OH (and also the other Si−O) bonds are elongated by only 0.01 Å. As a consequence of this nonuniform extension of the bond lengths, the Al−O(H)−Si bond angles become more acute, the decrease being 3.3° on average. On the other hand, quite surprisingly, the O−H bonds become slightly shorter if gradient corrections are applied. This indicates that the polarity of the chemical bond in the Al−O−H group is influenced by the gradient corrections, resulting in a stronger bond in the hydroxyl group. The energy difference between the most favorable and the least favorable acid site is about 0.28 eV. We have found a correlation between local geometry and energetics: Sites with larger intertetrahedral T−O−T angles can more easily adapt to the lattice distortions arising from the Si/Al substitution and protonation. The same correlation between a smaller T−O−T angle and an increased protonation energy has also been found in our recent study of Brønsted acid sites in gmelinite[61] and in earlier studies of cluster models for acid sites in zeolites.[31−33] On the other hand, the correlation between an increasing Al−O(H) bond length (and also the corresponding Si−O bond length in the nonprotonated structure) and an increasing energy of the acid site is less clear in mordenite than in gmelinite.

A possible interaction between acid sites has been studied for an increased Al/Si ratio (but respecting Löwenstein's rule excluding protonation of immediately neighboring tetrahedral sites). Except for the Al2−O3−H sites involving rather short proton−proton distances, such an interaction is found to be weak. However, it has to be pointed out that the short proton−proton distances characteristic for neighboring Al2−O3−H sites can occur quite frequently, if acid sites of different types are occupied simultaneously, even if Löwenstein's rule is respected. The part of our study that is most relevant to the catalytic activity of mordenite is the calculation of the O−H stretching frequencies and the investigation of the correlation between these frequencies and the distortions of the zeolitic framework introduced by the protonation. Because of the structural complexity of mordenite, our analysis had to be restricted to the most easily accessible acid sites where the OH groups are oriented toward the largest cavities. Both classical and quantum calculations have been performed, the quantum result leading to frequencies that are about 20 cm^{-1} higher. Because we have selected acid sites sharing certain structural characteristics, it is not surprising that the calculated frequencies fall into a rather narrow range: using the LDA, the anharmonic frequencies from the quantum calculation range between 3515 and 3567 cm^{-1}; the GGA leads to slightly higher frequencies ranging between 3552 and 3616 cm^{-1}. The GGA results centered around 3593 cm^{-1} agree very well with the main IR mode at 3606−3617 cm^{-1} attributed to Brønsted sites in the main channel, but one

has to admit that the range of calculated frequencies also extends to the low-intensity band at 3580−3590 cm^{-1} attributed to the less accessible acid sites in the side pockets.

Despite the small spread of the calculated frequencies, certain correlations between the geometry of the acid sites and the vibrational frequencies of the hydroxyl group are recognizable. The essential point is that a wider intertetrahedral T−O−T angle not only facilitates Si/Al substitution and protonation, it also leads to a lower O−H frequency and hence, according to common lore, also to a higher reactivity of the acid site. However, it should be kept in mind that our analysis does not cover the less accessible sites in the smaller cavities. Some of these sites (O4, O9) have large T−O−T angles. Hence, if the correlation we have pointed out holds, this would explain the origin of the low-frequency component in the IR spectra, but this remains to be confirmed. Also the reactivity of the acid site should be investigated by the adsorption of test molecules.

In summary, our work demonstrates that extended LDF studies on periodic systems are now feasible for quite large zeolites and allows new insight to be gained into their structural and chemical properties.

Acknowledgment. This work has been performed within the Groupement de Recherche Européen (GdR-E) "Dynamique moléculaire quantique appliquée à la catalyse", supported by the Centre National de la Recherche Scientifique (CNRS), the Institut Français du Pétrole (IFP), and TOTAL Raffinage Distributions. We thank IDRIS (Orsay) for the generously allocated computer time. Fruitful discussions with Y. Jeanvoine and J. G. Ángyán are gratefully acknowledged.

Supporting Information Available: Tetrahedral deformation parameters for all three different cases (i.e., pure-silica, sodium-exchanged, and protonized mordenite), definition of the tetrahedral parameters, and statistical distribution of the T−O bond lengths and O−T−O angles in pure-silica and sodium-exchanged mordenite. This material is available free of charge via the Internet at http://pubs.acs.org.

References and Notes

(1) Catlow, C. R. A., Ed. *Modelling of Structure and Reactivity in Zeolites*; Academic: London, 1992.
(2) Dyer, A. *An Introduction to Zeolite Molecular Sieves*; Wiley: Cluchester, 1988.
(3) Stave, M. S.; Nicholas, J. B. *J. Phys. Chem.* **1993**, *97*, 9360.
(4) Sauer, J.; Horn, H.; Häser, M.; Ahlrichs, R. *Chem. Phys. Lett.* **1990**, *173*, 26.
(5) Haase, F.; Sauer, J. *J. Am. Chem. Soc.* **1995**, *117*, 3780.
(6) Derouane, E. G.; Fripiat, J. G. *J. Phys. Chem.* **1987**, *91*, 145.
(7) Shah, R.; Gale, J. D.; Payne, M. C. *Science* **1996**, *271*, 1395; *J. Phys. Chem.* **1996**, *100*, 11688; *Phase Transitions* **1997**, *61*, 67.
(8) Jeanvoine, Y.; Ángyán, J. G.; Kresse G.; Hafner, J. *J. Phys. Chem.* **1998**, *102*, 5573.
(9) Nusterer, E.; Blöchl, P. E.; Schwarz, K. *Angew. Chem., Int. Ed. Engl.* **1996**, *35*, 175.
(10) Campana, L.; Selloni, A.; Weber, J.; Goursot, A. *J. Phys. Chem.* **1995**, *99*, 16351.
(11) Campana, L.; Selloni, A.; Weber, J.; Goursot, A. *J. Phys. Chem.* **1997**, *101*, 9932.
(12) Jeanvoine, Y.; Ángyán, J. G.; Kresse, G.; Hafner, J. *J. Phys. Chem.* **1998**, *102*, 7307.
(13) Termath, V.; Haase, F.; Sauer, J.; Hutter, J.; Parrinello, M. *J. Am. Chem. Soc.* **1998**, *120*, 8512.
(14) Kessi, A.; Delley, B. *Int. J. Quantum Chem.* **1998**, *68*, 135.
(15) Apra, E.; Dovesi, R.; Freyria-Fava, C.; Pisani, C.; Roetti, C.; Saunders: V. R. *Model. Simul. Mater. Sci. Eng.* **1993**, *1*, 297.
(16) Teunissen, E. H.; Roetti, C.; Pisani, C.; de Man, A. J. M.; Jansen, A. P. J.; Orlando, R.; van Santen, R. A.; Dovesi, R. Model. *Simul. Mater. Sci. Eng.* **1994**, *2*, 921.
(17) White, J. C.; Hess, A. C. *J. Phys. Chem.* **1993**, *97*, 6398.
(18) White, J. C.; Hess, A. C. *J. Phys. Chem.* **1993**, *97*, 8703.
(19) Janssens, G. A. O.; Baekelandt, B. G.; Toufar, H.; Mortier, W. J.; Schoonheydt, R. A. *J. Phys. Chem.* **1995**, *99*, 3251.
(20) Meier, W. M. *Z. Kristallogr.* **1961**, *115*, 439.
(21) Gramlich, V. Doctoral Thesis, No. 4633, ETH Zürich, 1971.
(22) Alberti, A.; Davoli, P.; Vezzalini, G. Z. *Kristallogr.* **1986**, *175*, 249.
(23) Minachev, V.; Garamin, V.; Isakova, T.; Kharamov, V.; Bogondo, V. *Adv. Chem.* **1977**, *102*, 441.
(24) Mortier, W. J.; Pluth, J. J.; Smith, J. V. *Mater. Res. Bull.* **1976**, *11*, 15.
(25) Schlenker, J. L.; Pluth, J. J.; Smith, J. V. *Mater. Res. Bull.* **1979**, *14*, 751.
(26) Schlenker, J. L.; Pluth, J. J.; Smith, J. V. *Mater. Res. Bull.* **1979**, *14*, 849.
(27) Shiokawa, K.; Ito, M.; Itabashi, K. *Zeolites* **1989**, *9*, 170.
(28) Ito, M.; Saito, Y. *Bull. Chem. Soc. Jpn.* **1985**, *58*, 3035.
(29) Mortier, W. J.; Pluth, J. J.; Smith, J. V. *Natural Zeolites Occurrence, Properties, Use*; Pergamon Press: Elmsford, NY, 1978.
(30) Schlenker, J. L.; Pluth, J. J.; Smith, J. V. *Mater. Res. Bull.* **1978**, *13*, 169.
(31) van Santen, R. A.; Kramer, G. J. *Chem. Rev.* **1995**, *95*, 637.
(32) Toulhoat, H.; Clemendot, S. *Rev. IFP* **1996**, *51*, 49.
(33) Redondo, A.; Hay, P. J. *J. Phys. Chem.* **1993**, *97*, 11754.
(34) Kresse, G.; Hafner *J. Phys. Rev. B* **1993**, *48*, 13115.
(35) Kresse, G.; Hafner, *J. Phys. Rev. B* **1994**, *49*, 14251.
(36) Kresse, G.; Furthmüller, J. *Computat. Mater. Sci.* **1996**, *6*, 15; *Phys. Rev. B* **1996**, *54*, 11196.
(37) Perdew, J. P.; Zunger, A. *Phys. Rev. B* **1981**, *23*, 5048.
(38) Ceperley, D. M.; Alder, B. J. *Phys. Rev. Lett.* **1980**, *45*, 566.
(39) Perdew, J. P.; Chevary, J. A.; Vosko, S. H.; Jackson, K. A.; Pedersen, M. R.; Singh, D. J.; Fiolhais, C. *Phys. Rev. B* **1992**, *46*, 6671.
(40) Perdew, J. P.; Wang, Y. *Phys. Rev. B* **1992**, *45*, 13244.
(41) Blöchl, P. E. *Phys. Rev. B* **1994**, *50*, 17953.
(42) Kresse, G.; Joubert, D. *Phys. Rev. B* **1999**, *59*, 1758.
(43) Vanderbilt, D. *Phys. Rev. B* **1990**, *41*, 7892.
(44) Kresse, G.; Hafner, J. *J. Phys.: Condens. Matter* **1994**, *6*, 8245.
(45) Demuth, T.; Jeanvoine, Y.; Hafner, J.; Ángyán, J. G. *J. Phys.: Condens. Matter* **1999**, *11*, 3833.
(46) Teter, D. M.; Hemley, R. J.; Kresse, G.; Hafner, J. *Phys. Rev. Lett.* **1998**, *80*, 2145.
(47) Senchenya, I. N.; Garrone, E.; Ugliengo, P. *J. Mol. Struct.: THEOCHEM* **1996**, *368*, 93.
(48) Ugliengo, P. ANHARM−A program to solve numerically the mononuclear Schrödinger equation (unpublished).
(49) Gibbs, G. V. *Am. Mineral* **1982**, *67*, 421.
(50) Petrovic, I.; Navrotsky, A.; Davis, M. E.; Zones S. I. *Chem. Mater.* **1993**, *5*, 1805.
(51) Derouane, E. G.; Fripiat, J. G. *Proc. Sixth Int. Zeolite Conf.* **1983**, 717.
(52) Löwenstein, W. *Am. Miner.* **1954**, *39*, 92.
(53) Alberti, A. *Zeolites* **1997**, *19*, 411.
(54) Fujino, T.; Kashitani, M.; Fukuyama, K.; Kubota, J.; Kondo, J. N.; Wada, A.; Domen, K.; Hirose, C.; Wakabayashi, F.; Kano, S. S. *Chem. Phys. Lett.* **1996**, *261*, 534.
(55) Furuki, M.; Kubota, J.; Goto, Y.; Wakabayashi, F.; Kondo, J.; Wada, A.; Domen, K.; Hirose, C. *J. Electron Spectrosc.* **1993**, *64*, 259.
(56) Zholobenko, V. L.; Makarova, M. A.; Dwyer, J. *J. Phys. Chem.* **1993**, *97*, 5962.
(57) Bordiga, S.; Lamberti, C.; Geobaldo, F.; Zecchina, A.; Turnes-Palomino, G.; Otero Arean, C. *Langmuir* **1995**, *11*, 527.
(58) Wakabayashi, F.; Kondo, J.; Wada, A.; Domen, K.; Hirose, C. *J. Phys. Chem.* **1993**, *97*, 10761.
(59) Lercher, J. A.; Gründling, C.; Eder-Mirth, G. *Catal. Today* **1996**, *27*, 353.
(60) Garrone, E.; Kazansky, V. B.; Kustov, L. M.; Sauer, J.; Senchenya, I. N.; Ugliengo, P. *J. Phys. Chem.* **1992**, *96*, 1040.
(61) Benco, L.; Demuth, T.; Hafner, J.; Hutschka, F. *J. Chem. Phys.* **1999**, *16*, 7537.